Evaluation of the anti-glioma efficacy of Fucoidan in combination with Temozolomide: An experimental *in vitro, in silico and in vivo approach*

Synopsis of the thesis to be submitted for the award of the degree of Doctor of Philosophy
in

Inter-Disciplinary Research

(Faculty of Medicine)

Submitted to

SRI BALAJI VIDYAPEETH

Submitted by

Ms. Indrani Biswas
UIN: 1705003008

Under the guidance of

Dr. Anitha T.S

(Former Scientist- CIDRF, SBV),
Assistant Professor,
Department of Biochemistry and Molecular Biology, Pondicherry University,
Kalapet, Puducherry -605 014, India.

TABLE OF CONTENTS

1. INTRODUCTION 1

2. AIM AND OBJECTIVES 2

3. HYPOTHESIS 3

4. REVIEW OF LITERATURE 3

4.1 Glioma 3

4.2 Molecular pathology of Glioma 4

4.3 Glioblastoma multiforme (GBM) 4

4.4 Incidences and Epidemiology 5

4.5 Diagnosis and Treatment 5

4.6 Tumor relapse and the need for alternative therapies: Drug Repurposing 7

4.7 Molecular targets in Glioma 8

4.8 Disease models to study glioma 10

5. MATERIALS AND METHODS 11

5.1 Reagents 11

5.2 Cell lines and culture conditions 12

5.3 Cytotoxicity Assay 12

5.4 Calculation of Selectivity Index (SI) 13

5.5 Combination index analysis, normalized isobologram, and Fa-CI plot 13

5.6 Wound-healing assay 13

5.7 Haematoxylin and Eosin (H&E) Staining 14

5.8 Acridine orange/ ethidium bromide (AO/EtBr) dual staining 14

5.9 Nuclear Staining 14

5.10 Quantitative Real-Time PCR 15

5.11 Molecular Docking 16

5.11.1 Target retrieval **16**

5.11.2 Target preparation and active site prediction **17**

5.11.3 Ligand retrieval and Preparation **17**

5.11. 4 Molecular docking analysis **17**

5.12 Molecular dynamics simulation (MDS) **18**

5.13 Animals **18**

5.14 Intracranial tumor engraftment **18**

5.15 Animal Grouping **19**

5.16 Histopathological analysis of the dual-drug combination in glioma induced xenograft model **19**

5.17 Survival Analysis **20**

5.18 Toxicity studies **20**

5.19 Detection of Ultrastructural changes by Scanning Electron Microscopy (SEM) **20**

5.20 Immunohistochemistry Analysis **20**

5.21 **STATISTICAL ANALYSIS** **21**

6. RESULTS **21**

7. DISCUSSION **49**

8. SUMMARY & CONCLUSION **54**

9. REFERENCES **56**

10. PUBLICATIONS **63**

1. INTRODUCTION

Glioma, recognized as an "octopus tumor," stands out as one of the most lethal forms of central nervous system (CNS) tumor (1). The current standard-of-care for treating gliomas is the surgical removal of the tumour mass with approximately (20 weeks after survival). This is followed by radiotherapy (36 weeks of survival after radiation and surgery) and chemotherapy (40–50 weeks of survival) with a standard drug, temozolomide (TMZ) (2). Resistance to the medications has impeded their translation from bench to bedside despite the use of sophisticated systemic techniques.

In recent years, repurposing drugs has gained popularity as a desirable and cost-effective option to alternative therapies, which are more expensive and time-consuming to implement. Since repositioned pharmaceuticals have received Food and Drug Administration (FDA) approval, which lowers cost, this may improve the odds against the development of new glioma medications (3). Surprisingly, several of these repurposed medications are being tested in glioma patients, underscoring the significance of this therapeutic approach.

With a rising concern to screen potential drug leads for repurposing, epidemiological reports have stated that combining natural compounds with conventional radio and chemotherapy enhances the sensitivity of the standard drug and also alleviates therapy-associated complications in various cancers (4,5). Among them, marine natural products (MNPs) have proven to be effective biological modulators. These MNPs have been predominantly noted for their potent biological activities such as antimicrobial, anti-infective, anti-inflammatory, or anti-tumor activity (6,7). Thus, a plausible approach to utilize MNPs as a lead compound would accelerate the development of new anti-cancer drugs with increased efficiency and fewer side effects (8).

Fucoidan (FU), a sulfated polysaccharide derived from brown seaweeds, is a significant example of a MNP. In some regions of Northern Europe and Asia, the crude FU extracts are offered for sale as dietary supplements (9). In recent studies, there has been substantial emphasis on investigating the anti-tumor effects of FU in glioma as well as in lung, breast, colon and prostate cancers (10,11). Additionally, the combination of FU and cyclophosphamide dramatically reduced metastasis in the C57BL/6 Lewis lung cancer mouse model (11). As a single therapeutic alternative, FU has so far been shown to improve epigenetic differentiation by inhibiting tumour growth in glioma cells (12). Hitherto, the chemo-preventive potential of FU in glioblastoma remains unexplored. Based on the above lacuna, the present study was designed to gain novel insights on the anti-tumor and pro-apoptotic efficacy of FU, both alone and in combination with TMZ using *in vitro*, *in silico* and *in vivo* experimental model.

2. AIM AND OBJECTIVES

Aim: To investigate the anti-tumor efficacy of Fucoidan (FU) in combination with Temozolomide (TMZ) employing *in vitro*, *in silico* and *in vivo* experimental approaches

Objective I: To investigate the anti-proliferative effects of Fucoidan (FU) both individually and in combination with Temozolomide (TMZ) on modulating the inflammatory pathway in an *in vitro* experimental glioma model.

Objective II: To elucidate the interaction profiles of TMZ, FU and their active metabolites against the key drivers of inflammation in glioma by *in silico* analysis.

Objective III: To evaluate the anti-glioma effects of TMZ and FU, both individually and in combination in a sub-clinical orthotopic glioma-induced xenograft animal model.

3. HYPOTHESIS

The combination of two drugs, Temozolomide and Fucoidan, is anticipated to synergistically induce anti-proliferative and pro-apoptotic effects in glioma.

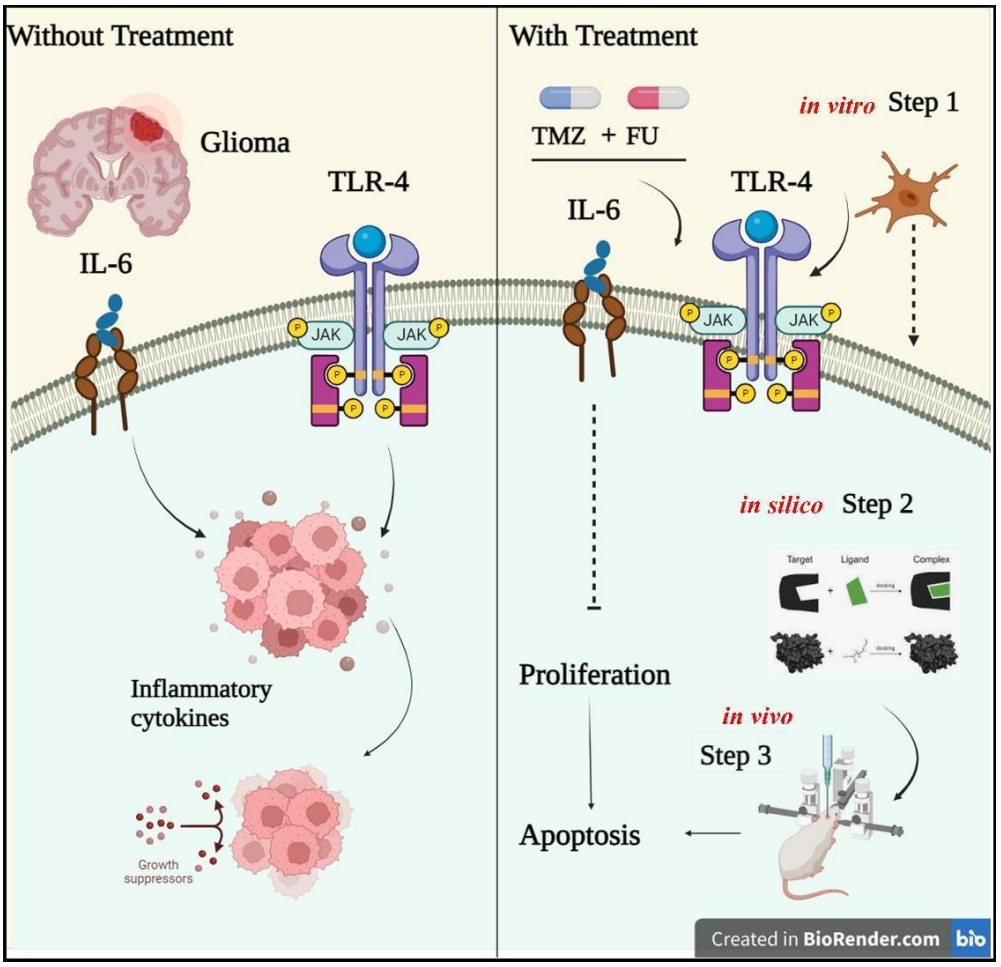

Figure 1: Schematic representation of the hypothesis

4. REVIEW OF LITERATURE

4.1 Glioma

CNS tumors have been regarded as the most lethal and aggressive tumors, leading to significant challenges in combating these malignancies (13). Among the prevalent types of CNS tumors, those originating from neurons are exemplified by medulloblastoma and primitive neuroendocrine tumors (PNET). Conversely, tumors arising from glial cells encompass glioma, glioblastoma multiforme (GBM), astrocytoma, ependymoma, and oligodendrogliomas (14). The majority of these tumors exhibited a minimal survival rate of approximately less than 12 months. In most cases, primary brain tumors like pilocytic astrocytoma's are less invasive and surgically manageable, as

opposed to gliomas or GBM. CNS tumors encompass wide range of symptoms and complications such as edema, nausea, headaches, seizures, fatigue, psychiatry disorders and other symptoms (15). Moreover, within and around the brain, the blood-brain barrier (BBB), consisting of an endothelial cell lining, presents a significant challenge for the transport of small molecules or drugs. Furthermore, each CNS tumor is characterized by a unique molecular aberration, posing challenges in successfully translating treatment strategies from bench to bedside (16). Brain tumors, classified into various types, exhibit unique cellular origins distinguishable by factors such as anatomical location, expression of cellular and molecular markers, and morphological resemblance to normal neuronal and epithelial cells (19). Among these CNS tumors, gliomas are particularly lethal due to their high recurrence and resistance rates. Currently, there is a shortage of studies addressing successful anti-glioma therapeutics with the potential for pharmacological advancements to combat gliomas.

4.2 Molecular pathology of Glioma

The term "glioma" serves as an umbrella, encompassing histological and pathological characteristics derived from various cell types, including astrocytes, oligodendrocytes, and neuro-epithelial cells. Gliomas can be categorized into different grades according to the WHO classification: Diffuse astrocytomas (grade I), anaplastic astrocytomas (grade III), and Glioblastoma multiforme (GBM, grade IV) representing distinct forms within the glioma spectrum (17). Genetic and molecular alterations through multi-step tumorigenesis lead to the development of primary and secondary high grade glioma, based on clinical, molecular and pathological characteristics. The complexity of tumor grading adds to the difficulty of achieving complete eradication of tumor growth (18). Glioma is commonly localized in four lobes namely, frontal, parietal and occipital and temporal region of brain, amongst which, the frontal lobe contributes to maximal percentage of this tumor growth. Examination of occurrence of these tumors by radiographic imaging such as Positron Emission Tomography (PET), Magnetic Resonance Imaging (MRI) to identify the extent of spread of tumor (19). Furthermore, the advancement in therapeutic approaches is influenced by factors such as genetics, behavior, environment, development and other inter-disciplinary subjects. The integration of these approaches enhances epidemiological studies aimed at mitigating the burden of disease (20).

4.3 Glioblastoma multiforme (GBM)

Glioblastoma multiforme (GBM), categorized as a grade IV glioma, is a rare condition that disproportionately affects men over women. However, the global incidence rate of GBM stands at 10 per 100,000 population across various

geographical locations, presenting a considerable clinical challenge (21). Some of the molecular attributes that pose challenges to combat GBM are-breaching BBB, tumor unresponsiveness to most of the chemotherapeutic agents and development of multi-drugs acquired resistance by these tumor cells (22). Primary GBM exhibits loss-of-heterozygosity (LOH) on chromosome 10 bearing phosphotensin homolog (PTEN), gene amplification of epidermal growth factor receptor (EGFR) or deletion mutation of EGFR to EGFRvIII, with enhanced activity of telomerase reverse transcriptase (TERT) activity (23).

4.4 Incidences and Epidemiology

The incidence rate of gliomas varies based on factors such as age, gender, and race. According to a Japanese study reported from 1989-2008, there was a rising trend in the number of individuals affected by gliomas. In addition, Chen *et al*. noted that the overall incidence rate for elderly patients was 13.16 per 100,000 (95% CI, 12.99-13.32) from 2000 to 2017 (27). The incidence rate was greater in males than in females. Additionally, the frontal and temporal lobes exhibited a higher incidence rate of GBM tumors. In an epidemiological study carried out in Malta, individuals diagnosed with GBM between 2008 and 2017 had an incidence ratio of around 1.4:0.9 per 100,000 people. About 58% of individuals aged 65 years and older from 2007 to 2017 received a diagnosis of GBM, highlighting an increasing concern within the aging population (28). Moreover, there have been reports indicating an elevated risk of GBM associated with radiation exposure, as observed in CT brain scans conducted over several years. In 2015, Hardell and Colberg documented an increased risk of glioma linked to the use of mobile phones, revealing an odds ratio of 3.0 (29). A 2016 study by Chien *et al*. reported that, although the incidence ratio between the United States and Taiwan was comparable, there was a higher occurrence of GBM in the Taiwanese population. Regional variations in both the incidence ratio and frequency of GBM have been documented, attributed to differences in lifestyle, ethnicity, race, and hereditary factors (24). Moreover, ionizing radiation exposure and genetic syndromes are widely recognized as risk factors associated with the development of GBM. Additionally, the various grades of GBM differ in terms of cellular morphology, clinical characteristics, biomarkers, and neuroimaging findings (25).

4.5 Diagnosis and Treatment

The standard-of-care diagnostic approach employs radiation to detect and assess the existence of tumorigenic lesions within and around specific locations. Consequently, imaging modalities like Magnetic Resonance Imaging (MRI), Computed Tomography (CT), Positron Emission Tomography (PET), and others have gained significant attention in the field of cancer diagnostics (26). Recently, implementation of these diagnostics has played a crucial role in

paving the way for the discovery of novel biomarkers in glioma. Notably, MRI enables identification and characterization of biological phenomena at molecular and cellular levels within living systems. Non-invasively introduced MRI probes facilitate the determination of target expression in tumors, serving as an indicator for evaluating the response of tumors to therapy (27). Radio-tracers like 18F-fluoro-2-deoxyglucose (18F-FDG) are extensively employed for the identification and localization of glioma stages, assessing the therapeutic effectiveness of FDA-approved drugs during recurrent phases of GBM. Additionally, some neurologic and oncologic biomarkers are utilized to elucidate the effectiveness of molecularly targeted inhibitors in glioma, including those targeting c-Met/PI3K/mTOR pathways and other receptor tyrosine kinases (RTKs) (28). Similarly, an alternative diagnostic imaging approach involves the use of PET-based radiotracers such as 18F-FDG, which was employed to assess tumorigenic responses to the anti-angiogenic agent, axitinib in a U-87MG induced xenograft model. Other radiotracers, such as 3-deoxy-3'-18F-fluorothymidine (18F-FLT) and 2-18F-fluoroethyl-triazolyl-conjugated (RGDyK) peptide (18F-FtRGD), are prevalent in estimating growth and proliferation rates by targeting the expression of enzymes like thymidine- 1-kinase during the early stages of tumor DNA synthesis (29). Previous studies have reported radiotracer ^{11}C-methyl-L-methionine (^{11}C-Met) is capable of effectively tracking alterations in proliferation and vessel remodeling within the initial stages, specifically within a time frame of less than 3 weeks. Currently, PET is widely utilized for various purposes, including assessing tumor invasion, contributing to differential diagnoses, onitoring post-treatment outcomes, and even aiding in the planning of surgical and radiotherapeutic interventions (30). Another alternative non-invasive imaging method is CT scan, which is considered as one of the preferable standards for diagnosing and detecting these tumors over other intracranial space-occupying lesions. Despite the progress made in traditional therapeutic modalities, there is a lack of effective treatment strategies, contributing to an ongoing and challenging battle against glioma (31). Beyond conventional treatment approaches, avenues for designing and implementing targeted drug delivery systems, such as nanoparticles (NPs) and nano-encapsulation bodies, as well as non-coding RNAs like siRNA, miRNA, or long non-coding RNAs (LncRNAs), chimeric antigen therapy (CAR), gene editing, and vaccine-based immunotherapies (38),have remain unexplored. For example, hyper-PEGylated hyperbranchedpolymers (HBPs) have emerged as promising therapeutic agents in several pre-clinical models, demonstrating minimal adverse effects. These HBPs exhibit an enhanced rate of permeability and retention (EPR) in brain tumors. A key factor in targeted drug delivery systems against the blood-brain barrier (BBB) is the regulated transport of small molecules across the barrier (39). The development of positively coated NPs may act as a trap to navigate the BBB, enabling the delivery of anti-glioblastoma drugs.

Similarly, Gregory *et al*. reported that solid polymer nanoparticles (SPNPs) containing siRNA against signal transducer and activation of transcription 3 factor (si-STAT3) demonstrated *in vitro* and *in vivo* downregulation of STAT3. This ultimately triggered tumor regression and long-term survival in mice models with induced glioblastoma, restoring elevated levels of immunological memory (40). It is observed that immune responses in various tumor types generate elevated responses, presenting a significant challenge in many tumors, including gliomas. Gliomas exhibit distinct immune escape mechanisms, making the development of targeted therapeutic regimens a complex task in navigating this intricate tug-of-war.

An alternative and revolutionary tool that has experienced substantial growth is "*in silico therapeutics,*" a concept that has garnered significant interest in the realm of computer-aided drug discovery (CADD). This approach involves virtual screening (VS) or molecular docking, serving as a foundational step in the design and development of therapeutics in the era of computational therapeutics (41). It acts as a preliminary analysis tool for screening potential pharmacological leads, particularly with a focus on anti-tumor therapeutics. In this context, artificial intelligence (AI) has taken a prominent role in various aspects of medical health, including diagnosis, prognosis, and therapy across different diseases, particularly in cancers like glioma. AI is broadly categorized into supervised and unsupervised machine learning (ML) (42). For example, Jin *et al*. highlighted that ML and deep learning (DL) tools have enabled the identification and quantification of tumor volume, as well as the segmentation of tumor regions for downstream analysis. Additionally, AI has proven instrumental in identifying tumor types or grades, molecular subtypes, genetic mutations, predicting patients' treatment response, survival, prognosis, or relapse (42). Furthermore, AI has facilitated the development of biomarkers based on neuronal imaging and tumor radiomics. Despite several breakthroughs in AI, its successful translation from bench to bedside for the strategic development of anti-glioma therapeutics remains a challenge (43).

4.6 Tumor relapse and the need for alternative therapies: Drug Repurposing

Glioma exhibits rapid recurrence and tumor relapse, which succumbs the progression free and overall survival rate of patients. Molecular pathogenesis of glioma is extensive, which necessitates the dire need to implement some of the alternative therapies such as drug repositioning or repurposing (32). Drug repurposing refers to the usage of already existing drugs with known pharmacological profile and acquired FDA approval. In the past few decades, drug repurposing has emerged as one of the therapeutic spotlight in the field of drug discovery (4). TMZ is one of the standard-of-care of treatment for glioma,

however, being the most outrageous form of CNS malignancies it presents a significant challenge in the form of acquired drug resistance (ADR) (33). TMZ mediates its sensitivity via methylation of O^6 at guanine residue in the promoter region of methyl guanine methyl transferase (MGMT) gene. Glioma cells have acquired resistance to TMZ, leading to an enhanced propagation of the tumor (34). In recent years, natural compounds have arisen as potentiating anti-tumor agents in combination with TMZ against several cancers including glioma.

As an instance, curcumin, a polyphenolic compound extracted from rhizome of *Curcuma longa*, has garnered wide range of bioactivities including anti-cancerous. Emerging study findings suggest that curcumin exerts chemo-preventive, anti-proliferative, anti-invasive and anti-angiogeneic, indicating the fact that it might exert significant anti-neoplastic effects. In continuation with these findings, it was reported that curcumin arrested cell growth, survival, proliferation possibly via downregulation of JNK/NF-κB or PI3K/AkT/mTOR or Janus Kinases (JAK)/STAT3 signaling ailments in GB cells. Additionally, curcumin exerted apoptosis via cell cycle arrest such as G1/S or G2/M, alternatively, it enhanced expression of p53/p21 and downregulated expression of cyclin-D1 in U-87MG human glioblastoma cells (35). Similarly, epigallocatechin gallate (EGCG), is one of the prime polyhenolic compound present in green tea, is known to exert chemo-sensitive and chemo-preventive properties in combination with synthetic compounds such as 5-fluorouracil, taxol or gemcitabine, against wide range of malignancies *in vitro* and *in vivo* experimental models (36). Likewise, Resveratrol, is a polyphenolic compound abundantly available in fruits and vegetables, has exerted anti-tumor activities against several cancer cell lines including glioma, explicitly. As an instance, *Sato et al* reported that Reveratrol provoked proteasomal degradation of Nanog (a essential factor to trigger formation of stem cells) and activation of p53, concurrently, thereby promoted differentiation of glioma stem cells (37).

4.7 Molecular targets in Glioma

Glioma exhibits aggressive tumor growth, owing to the presence of molecular aberrations involved in cellular growth and proliferation- Phosphatidyl inositol-3-kinase/mammalian or mechanistic target of rapamycin (PI3K/AKT/mTOR), JAK/STAT3, RAS/RAF, Wnt/β-catenin, Interleukin -6 (IL-6)/Toll like receptor 4 (TLR-4) pathway (38). In glioma, among all these pathways, inflammatory signaling cascades play a crucial role in promoting, progressing, and expanding the tumor. Most of the CNS malignancies including glioma exhibit a compromised immune-surveilling tumor microenvironment, which promotes tumor progression (39). Inflammation is a bi-directional player in most of the cancers including glioma. Immune cells within the CNS release various factors, primarily cytokines or chemokines such as transforming growth factor-beta

(TGF-β), that are capable of either triggering or inhibiting tumorigenesis (39,40). Furthermore, apart from the resident macrophages of CNS, microglial cells exhibit similar characteristics to infiltrating macrophages that invade through the BBB under abnormal conditions like trauma, stroke, and CNS malignancies (54). The intricate interplay between these immune cells and tumor cells adds an additional layer of complexity, contributing to the prolonged nature of this ongoing battle.

The inflammatory signaling pathway is aberrantly activated across various cancer types, including breast, colon, liver, lungs and brain, and is modulated by interleukins (IL) and chemokines/cytokines such as IL-6,7,8 and TLR1-11. IL-6/TLR4 coordinates with interferon-γ (IFN-γ), a pivotal molecule initiating the innate immune response (41). Parallelly, the process of tumorigenesis is transduced through the modulation of Janus Kinase/Signal transducer activated transcription factor 3 (JAK/STAT3), which are key transcription and signaling parameters that together promotes tumor cell survival, growth and proliferation in glioma (42). This transduction process is influenced by one of the free radical generating species, nitrogen oxygen synthase 2 (NOS2). Elevated expression of NOS2 is associated with a poor prognosis in glioma patients. NOS2 exacerbates the process of tumor heterogeneity, thereby promoting gliomagenesis (43). All of the signature molecules of inflammation, including IL-6/TLR-4 and JAK/STAT3 following IFN-γ and NOS2 activation, stimulate glioma promotion and progression.

One of the key contributor to the facilitation of glioma promotion is mediated through the evasion of programmed cell death, also known as apoptosis. Apoptosis, a form of programmed cell death, is carried out by a family of cysteine-aspartate residue proteases called caspases, which perform various functions based on the mode of activation initiator and executioner caspases. Executioner caspases, such as caspase 3 and 9, lead to the activation of apoptotic protease activating factor (Apaf), consequently leading to the formation of the apoptosome, ultimately resulting in cell death (44). Unlike other cancer cells, glioma employs a unique mechanism to circumvent tumor antigen presentation, preventing immune cells from sensitizing its destruction. Alternatively, these tumor cells exhibit distinct mechanisms to evade immune surveillance, often by silencing the expression of tumor suppressor proteins such as p53 and retinoblastoma (Rb), which, under normal circumstances, regulate controlled cell proliferation (59). This classic phenomenon presents an intriguing and appealing target for anti-tumor therapeutics.

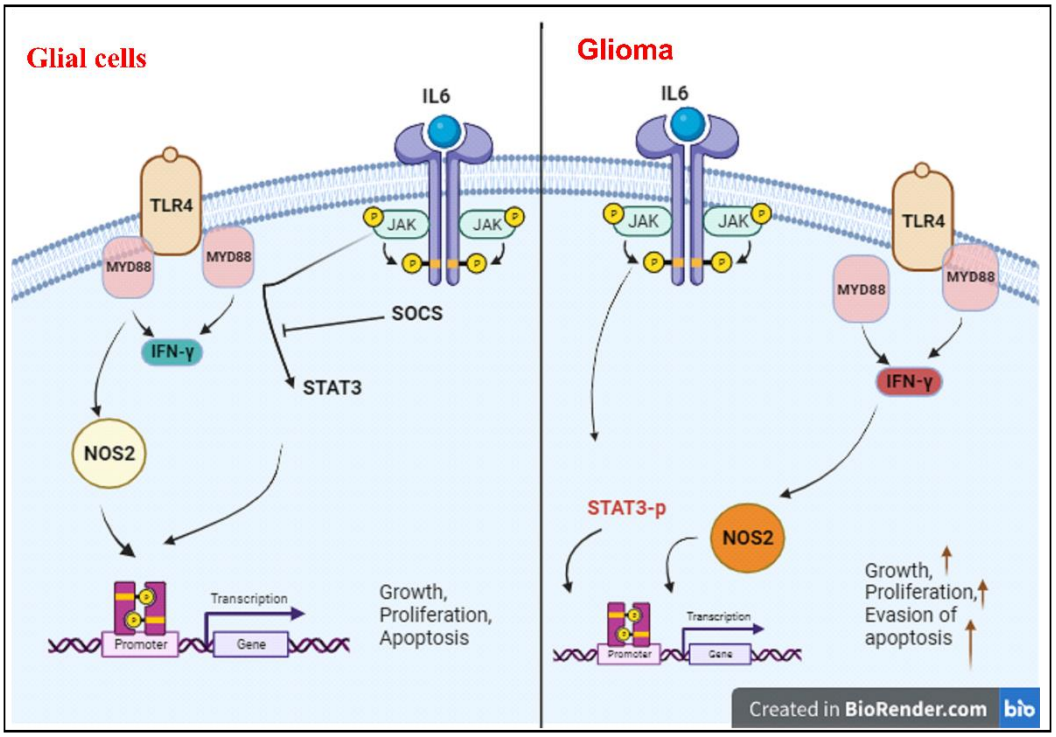

Figure 2: Proposed mechanism of switching-IL6/TLR4 and JAK/STAT3 signaling cascades in normal glial cell and glioma.

4.8 Disease models to study glioma

Tumor cells within glioma constitutes a complex tumor microenvironment, which necessitates to implement experimental models or set-ups in order to unravel the intricate molecular pathogenesis of this disease (45). Over the past few decades, the emergence of *in silico*-based strategies has served as a preliminary step to screen numerous therapeutics using CADD tools, mainly docking. Subsequently, evaluating the stability of the docked complexes against the targets becomes an essential endpoint prerequisite (46). Furthermore, the validation of *in silico*-screened compounds needs to be assessed in *in vitro* and *in vivo* models to determine their potential pharmacological activities.

Due to the profound molecular heterogeneity of glioma, *in vitro* experimental models could be employed to study genomic, transcriptomic, or proteomic related aberrations. All these parameters could be investigated using a 2D experimental setup deploying glioblastoma cell lines such as U-87 MG, LN-229, LN-18, and C6 (rat glioma cells) (62). Simultaneously, the use of experimental setups implementing TMZ- resistant cell lines-LN18,T98G, U138, CCF-STTG1, and U343-MG, is crucial to accurately assess the potential of anti-glioma pharmacological agents (47). Nevertheless, 2D experimental models

pose challenges concerning the spatio-temporal location of tumor formation and the elusive pathological features. This has led to the necessity to develop 3D experimental models, that facilitates to epitomize the role of tumor microenvironment and offers new perspective to underpin pathophysiological mechanisms in glioma. Based on this insight, brain organoids or mini-brains offer a potent tool for conducting *ex vivo* experiments, capturing intricate cellular and molecular mechanisms of various brain disorders or diseases, that ascribe parameters of human organ histology and pathology (48). Brain organoids developed for distinct sections such as forebrain, midbrain and hindbrain exhibit distinct molecular and cellular features that mimics the functional capacities of a naïve glioma (48). However, the implementation of *in vitro* experimental setups needs to be rigorously validated using *in vivo* experimental models. Some of the *in vivo* models include subcutaneous, intracranial and orthotopic xenograft tumor models, which are well-established models for investigating glioma histology and pathological features. This facilitates the unraveling of the underlying molecular pathogenesis in glioma development and progression (49).

Consistent with the aforementioned concept, this study aimed to assess the anti-glioma potential of FU and TMZ, both alone and in combination, using C6 rat glioma cells and an orthotopically induced glioma xenograft model. Moreover, to investigate the mechanism of action of these compounds, along with the active metabolites of TMZ (MTIC and AIC), against inflammatory targets-
IL-6, TLR-4, JAK, STAT3, IFN-γ, and NOS2, molecular docking was performed. Additionally, simulations were executed to predict the overall stability of each of these complexes.

5. MATERIALS AND METHODS

5.1 Reagents

Minimal Essential Medium Eagle (EMEM) (Catalogue No: AT047) and penicillin/streptomycin antibiotic solution were procured from Hi-Media, Mumbai. Fetal Bovine Serum (FBS), Pierce® RIPA buffer, DMSO and the drugs employed for the study namely, TMZ (Catalogue No: PHR1437), FU (active compound, Catalogue No: F8190 derived from *Fucus vesiculosus*) were obtained from Sigma Aldrich, USA. Polyclonal antibodies against IL-6 (Catalogue No. E-AB-A0286), TLR4 (Catalogue No. E-AB-A5258), JAK2 (Catalogue No. E-AB- A7694), STAT3 (Catalogue No. E-AB-A11216), IFN-γ (Catalogue No. E-AB-A12450), NOS2 (Catalogue No. E-AB-A14031) and goat anti-rabbit IgG-HRP secondary antibody (Catalogue No: E-AB-AS014) were purchased from Elabscience Biotechnology Inc, Hubei, China.

5.2 Cell lines and culture conditions

C6 rat glioma cell line (RRID: CVCL_0194; Passage number- 48) and Human embryonic kidney transformed cell line (HEK293T; Passage number-10) was obtained from National Centre for Cell Sciences (NCCS), Pune, India. C6 and HEK293T cells were maintained at 37℃ under 5% CO_2 in nutrient mixture Ham's F12 media and Dulbecco's Modified Eagle's medium (DMEM), respectively, supplemented with 10% FBS and 1% antibiotic solution (100 U/ml penicillin and 100 µg/ml streptomycin), respectively. At the rate of 80% confluence, cells were seeded in 6-well, 24-well, or 96-well plates based on the experiments being performed. Stock solutions of TMZ and FU were prepared in dimethyl sulfoxide (DMSO) and water. The aliquots were stored at -20ºC. On the day of the experiments, FU and TMZ were dissolved in the culture medium, in which the final concentration of DMSO was less than 0.1 (%v/v).

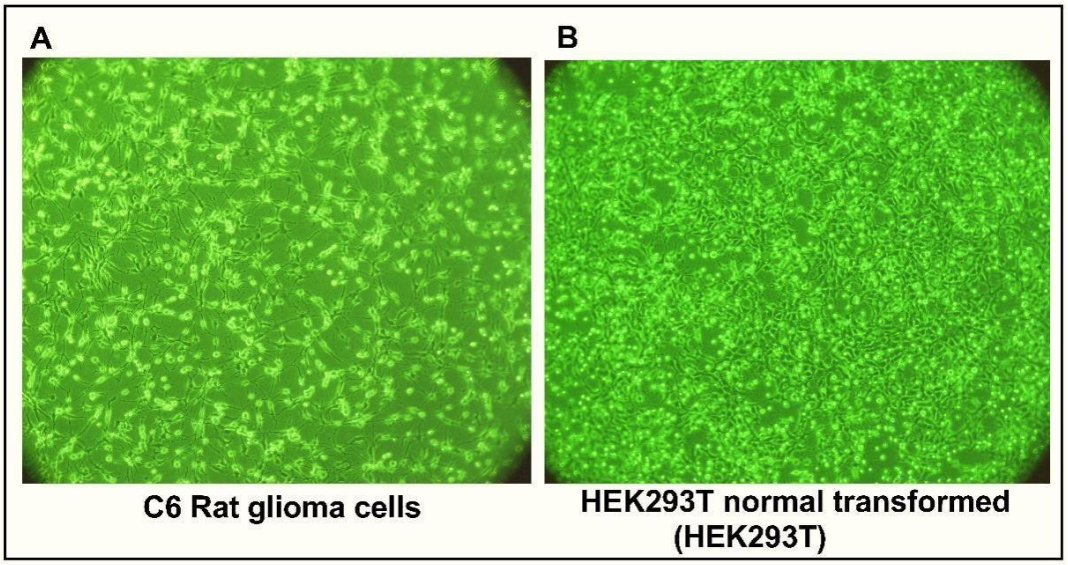

Figure 3: Phase contrast microscope images of (A) Rat glioma cells-C6 and (B) Human embryonic kidney 293 transformed (HEK293T) cells at 10X magnification

5.3 Cytotoxicity Assay

The cytotoxicity of the drugs, either alone or in combination was assessed using MTT on C6 and HEK293T cell lines. Briefly, C6 and HEK293T cells were seeded in a 96-well plate at a density of $5x10^3$ cells/well and incubated for 24 hours. Cells were then treated with TMZ and FU at working concentrations of 10, 50, 100, 150, 200, 250, 300 µM and cytotoxicity was assessed 24 hours post-treatment. Based on the IC_{50} values of the individual drug-treated cells, TMZ (IC_{20}: 1.2 µM) was combined with varying concentrations of FU (10, 50, 100, 150, 200, 250, 300 µM). After 24 hours of dual-drug treatment,

media was discarded completely and 20 µl of 5 mg/ml MTT was added to each well and incubated at 37℃ for 3 hours. The purple-coloured formazan crystals formed were dissolved in 180 µl of DMSO. Absorbance was read at 570 nm spectrophotometrically (Molecular Devices Spectra-Max M5, USA). The absorbance value of untreated control cells was fixed at 100%. The experiment was repeated at least three times. The cytotoxicity was calculated using the formula:

Cytotoxicity = [(Optical density {OD} of treated cell − OD of blank)/ (OD of control − OD of blank) × 100].

5.4 Calculation of Selectivity Index (SI)

To determine the selectivity and specificity of TMZ, FU, and their combination on glioma cells, SI was calculated using the following formula: SI= (IC_{50} of the individual and dual-drugs on HEK293T)/ (IC_{50} values obtained for the same treatment regimen on C6 glioma cells). A higher SI value indicates more selective and sensitivity towards cancer cells of the probed drugs and their combination.

5.5 Combination index analysis, normalized isobologram, and Fa-CI plot

The statistical Combinatorial Drug Index (CI) was calculated to analyze the interaction pattern of the drugs, while the Chou-Talalay method was used to determine the CI value. The CI values were calculated manually using the CI equation: CI=(D)1/(Dx)1+(D)2/(Dx)2, where (Dx)1 and (Dx)2 represents the dose of drug 1 and drug 2 in a combination which is required to attain the same efficacy as that of drug 1 (D1) and drug 2 (D2), when used alone. According to the Chou-Talalay method, the following criteria of drug-drug interactions were considered by CI: synergistic effect, CI < 1; additive effect, CI = 1; antagonist effect of drugs, CI > 1. Further, Dose-effect curve, CI, Fa-CI and Drug receptor index (DRI) plots were generated using Compusyn software.

5.6 Wound-healing assay

To determine the effect of the drugs on the inhibition of glioma migration, C6 cells were plated at a density of $4x10^5$ in 6-well plates. At 90% confluence, using a 200 µl sterile plastic tip, a scratch was made on the monolayer of cells. The peeled-off cells were washed using 1X Phosphate Buffered Saline (1X PBS) and thereafter the cells were maintained in a 2% FBS medium. Following, the cells were treated with the indicated concentration of the drugs both individually and in combination for 24 hours. Cell scratch spacing was evaluated at 0 and 24 hours by calculating the cell mobility (50).

5.7 Haematoxylin and Eosin (H&E) Staining

To detect the induction of apoptotic changes at the morphological level, H & E staining was carried out (51). For this, $3x10^5$ C6 cells were seeded in sterile coverslips in a 30 mm dish. Following 24 hours, cells were treated with the respective IC_{50} values of the drugs for 24 hours. Post-incubation, the medium in each dish was discarded, followed by fixation of cells using 4% paraformaldehyde for 10 mins at room temperature. H &E stain was then performed and the cells were imaged at 40x magnification under a light microscope (Zeiss Light Microscope, Germany). Densitometry analysis was performed using Image J.

5.8 Acridine orange/ ethidium bromide (AO/EtBr) dual staining

To further validate the changes associated with apoptosis at the morphological level, acridine orange/ ethidium bromide (AO/EtBr) dual staining was performed (52). C6 cells were seeded in a 24-well plate at a density of $20x10^3$/well and were then treated with the drugs, both individually and in combination for 24 hours at 37℃. Following incubation, cells were washed with 1X PBS and stained with 5 µl of 100 µg/ml AO and 100 µg/ml EtBr at room temperature for 5 minutes. Stained cells were subsequently observed and imaged under a fluorescent microscope (Axiovert 40 CFL, Germany) with an excitation wavelength of 300-360 nm. The number of apoptotic cells per field was counted, and the apoptosis rate was calculated as:

% apoptotic cells = number of apoptotic cells/total number of cells ×100, following quantification using ImageJ software.

5.9 Nuclear Staining

To synchronously confirm the apoptosis induction effect of the drugs at the nuclear level, the fluorescent nuclear stain, 4'6, Diamidino-2-Phenyl Indole (DAPI) was employed (53). To carry out DAPI staining, C6 glioma cells were seeded at a density of $15x10^3$ cells/well and treated with the respective IC_{50} value of the drugs. After 24 hours' post-treatment, the cells were washed with 1X PBS followed by fixation in 4% paraformaldehyde for about 10 minutes at room temperature. After fixation, the cells were permeabilized using 0.1% Triton X-100 followed by incubation with 1 µg/ml of DAPI in the dark. Stained cells were subsequently observed and imaged under a fluorescent microscope (Axiovert 40 CFL, Germany) with an excitation wavelength of 359 nm. The percentage of apoptosis was evaluated using ImageJ software.

5.10 Quantitative Real-Time PCR

To quantitatively assess the mRNA transcript levels of inflammatory and pro-apoptotic markers, quantitative Real-Time PCR (qRT-PCR) was performed. Briefly, total RNA from all of the experimental groups was isolated using RNAiso Plus (Takara, Japan). Complementary DNA (cDNA) was synthesized with the HiMedia-cDNA Synthesis Kit (HiMedia, India). qRT-PCR was performed using CFX96 thermocycler (Bio-Rad, Hercules, California, USA) and SYBR Green (Takara, Japan) to detect the mRNa. The reaction conditions were as follows: Initial denaturation: 95℃ for 30 seconds; followed by 39 cycles of denaturation at 95℃ for 10 seconds; annealing at a primer-specific annealing temperature for 30 seconds. The relative gene expression was calculated with the $2^{-\Delta\Delta C_t}$ method, where:

$\Delta C_t = (C_{t\ target\ gene} - C_{t\ GAPDH})$ sample- $(C_{t\ target\ gene} - C_{t\ target\ gene})$ control calibrator. The primers were designed using the primer BLAST tool and are listed in Table 1.

Table 1: Primers designed for each gene

Sl No	Genes	Forward Primer (5'->3')	Reverse Primer (5'->3')	Annealing Temperature (℃)
1.	IL-6	CTGGTCTTCTGGAGT TCCGT	TGGTCTTGGTCCTTA GC CAC	62
2.	TLR-4	TCTGCCCTGCCACCA TTTAC	GGAAGTACCTCTAT GC AGGGAT	64
3.	IFN-γ	ATGGATGCTATGGA AGGAAAGAG	CACTTATGTTGTTGC TG ATGGC	58
4.	STAT3	TGGGTCTGGCTAGA CAAT	TCGTTGGTGTCACAC A GAT	58
5.	NOS2	TCGTTGGTGTCACAC AGAT	CGGCTGGACTTCTCA CT CTG	60
6.	MYD88	CGACGCCTTCATCTG CTACT	ACCATGCGACGACA CC TTTT	54
8.	Caspase -3	GGCCGACTTCCTGTA TGCTT	GGCCGACTTCCTGTA TG CTT	60
7.	GAPDH	TCTCTGCTCCTCCCT GTTCTA	TACGGCCAAATCCG TT CACA	55

5.11 Molecular Docking

5.11.1 Target retrieval

Target retrieval was performed for six major proteins of inflammatory pathway namely IL-6, TLR-4, JAK2, STAT3, IFN-γ, and NOS2 from Uniprot (http://ca.expasy.org/sprot/).
The 3D structure obtained from PDB was used for further analysis. The details of the targets are listed in Table 2.

Table 2: List of targets retrieved from Uniprot and PDB

Sl. No	Protein Name	Function	PDB ID	Structure Resolution (Å)
1.	IL-6	Pro-inflammatory cytokine involved in innate immune response.	2L3Y	2.16
2.	TLR-4	Cooperates with lipopolysaccharide (LPS) to mediate the innate immune response.	2Z64	2.84
3.	IFN-γ	Belongs to class of interferon family, aids in immunogenic response against foreign antigens, thereby activating effector immune cells and enhancing antigenic presentation.	1FYH	2.04
4.	JAK2	Involved in various processes such as cell growth, development, and differentiation or histone modifications. Also involved in innate and adaptive immunity.	2HDX	2.35
5.	STAT3B	Mediates cellular responses to interleukins and also acts as a regulator of inflammatory responses.	1BG1	2.25
6.	NOS2	Messenger molecule with diverse functions, such as generation of nitric oxide and serves as a secondary messenger. It can mediate tumoricidal activity in macrophages.	3NQS	2.20

5.11.2 Target preparation and active site prediction

The 3D structure of six targets was imported individually into the maestro and were prepared using protein preparation wizard of the Schrodinger suite (Schrödinger Release 2019–4: Maestro, Schrödinger, LLC, New York, NY, 2019). The receptor preparation process includes: modelling of missing residues and missing side chains, the addition of missing hydrogen atoms, correcting the missing atoms in residues, redundancy validation in occupancies of atoms, modification of metal ionization states and assigning proper charges, removal of undesired water molecules and ideal protonation state of histidine. The presence of negatively and positively charged amino acid residues, facilitates to interact with the surrounding moieties across the ligand-protein complex, thereby rationalizing the presence of these three residues specifically, namely Arg, Gln and His. These amino acid residues of the drug targets were potentially spun to facilitate hydrogen and other non-bonded interactions, across the ligand-protein complexes with the surrounding moieties. The receptors were optimized using OPLS-3e force field and subsequently minimized to relax the bond angles, lengths and associated clashes (54). After preparation for all the six targets, the binding site information, which is used for the prediction of protein-ligand interactions, was collected using sitemap protocol (Schrodinger suite).

5.11.3 Ligand retrieval and Preparation

The ligands selected for this study were TMZ, FU from *Fucus vesiculosus*, 5-(3-Methy1-trizeno)-imidazole-4-carboxamide (MTIC) and 4-amino-5-imidazole-carboxamide (AIC). TMZ being a pro-drug, at physiological pH is rapidly hydrolyzed into the active form of the drug, MTIC. This subsequently gets metabolized to produce the final degradation product of TMZ, AIC. The 3D structures of ligands, TMZ, FU, MTIC and AIC were retrieved from Pubchem. The retrieved files were converted into .pdb format using Pymol. All the compounds were imported individually into maestro and were prepared using LigPrep module (Schrödinger Release 2019–4: Maestro, Schrödinger, LLC, New York, NY, 2019).

5.11. 4 Molecular docking analysis

The Glide XP (extra precision) docking method was used to predict the binding effectiveness of compounds in the active site of targets (Schrodinger suite) using Sitemap protocol as listed in Table 4. The prepared targets and ligands were given as input for glide docking and the grid box was produced utilizing the receptor grid generation procedure (Schrodinger suite) to delineate the docking area in the protein, which allows for more accurate ligand binding scoring. The simulations of molecular docking were run with default

parameters (55). The docking score, glide energy and number of hydrogen bond (HB) contacts between the target and the ligand were used to validate the simulation results.

5.12 Molecular dynamics simulation (MDS)

The structural and dynamic changes accompanied with each of the protein-ligand complexes were analyzed using molecular dynamics simulation. The simulation was executed with Gromacs 5.1.4 suite (56) with GROMOS96 43a1 force field on LINUX workstation. Gromacs provides high molecular simulation results and has been considered as a standard reference tool for simulation in comparison to Desmond. During the initial stage, system relaxation was performed to eliminate unwanted atomic contacts, which may lead to unstable MD simulation. Each of the protein-ligand complexes was solvated in a cubic simulation box under a Simple Point Charge 216 (SPC 216) water environment. There was a free run for 10 ps under the equilibrium period with a force constant of 1000 kJ mol−1 mol−2. Following energy minimization, the system was equilibrated with reference temperature of 300K at constant temperature and volume (NVT). Further, pressure was maintained with reference pressure of 1 bar at constant temperature and constant pressure (NPT). Temperature was controlled by V-rescale, a modified approach for Berendsen temperature coupling method. The minimized structures were subjected to MD simulation for 20000 picoseconds (ps) without restrictions. Analysis for MD simulation was executed in terms of the following: Root Mean Square Deviation (RMSD), Root Mean Square Fluctuation (RMSF), Solvent Accessible Surface Area (SASA) and Radius of Gyration (Rg) (57).

5.13 Animals

Healthy male Wistar rats (180-240 grams; 8-10 weeks old, n=40) were purchased from Tamil Nadu University of Veterinary Animal Sciences (Tamil Nadu, India) and were maintained under optimum humidity (50-60%), temperature (22±1ºC) and light conditions (12 hours light-12 hours dark cycle), with pellet food and water provided *ad libitum*. All the animal experiments carried out in the study were in compliance with ethical standards and approved by the Institutional Animal Ethics Committee (IAEC No: 03/IAEC/MG/09/2021-II). Experiments were conducted based on the Control and Supervision of Experiments on Animals (CPCSEA) and Animal Research: Reporting of *In Vivo* Experiments (ARRIVE) guidelines.

5.14 Intracranial tumor engraftment

To orthotopically implant glioma cells into healthy rats, stereotactic surgery was carried out according to the protocol (58). For this, the xenograft recipient

was sedated using ketamine and xylazine cocktail (87 mg/kg and 13 mg/kg body weight). The skull was exposed by incising the skin from the frontal to the occipital bone. After marking the implantation location (3.00 mm lateral and 0.5 mm posterior position), a small burr hole was drilled using a cordless power drill. Following, a total of 1×10^6 C6 cells suspended in 3 µl PBS was delivered into the target site at a depth of 6 mm. The burr hole was then sealed with bone wax and appropriate post-operative relief measures were carried out.

5.15 Animal Grouping

20 days post tumor implantation, the animals were randomly divided into five groups. Based on the previous literature (59,60), the dosage of the drugs was determined and was administered orally for 10 days.

Group I (Control rats, n=8): Healthy animals without tumor implantation or drug treatment.

Group II (Tumor-control rats, n=8): Glioma induced rats.

Group III (TMZ-treated rats, n=8): Glioma-induced, TMZ-treated rats administered with 50 mg/kg body weight of TMZ dissolved in 0.1% DMSO).

Group IV (FU-treated rats, n=8): Glioma induced, FU-treated rats administered with 50 mg/kg body weight of FU dissolved in distilled water).

Group V (TMZ+FU-treated rats, n=8): Glioma-induced, TMZ+FU-treated rats (administered with 15 mg/kg body weight of TMZ in 0.1% DMSO and 30mg/kg of FU dissolved in distilled water).

At the end of the treatment period, the rats from each experimental group were euthanized, brains were decapitated and stored in formalin or liquid nitrogen for further analysis. Additionally, vital organs (heart, lungs, liver, pancreas, spleen and kidney) were collected and stored in 10% formalin for histopathological evaluation.

5.16 Histopathological analysis of the dual-drug combination in glioma induced xenograft model

Brain tissues from each of the experimental groups were isolated and fixed in 10% formalin, embedded in paraffin and sectioned (4 µm). The tissue sections were stained using H & E and microscopic images of the stained sections were captured using Inverted microscope (Primo Star, Carl Zeiss, Germany) at 40x magnification followed by quantification using ImageJ software.

5.17 Survival Analysis

A survival study was conducted using a total of 24 animals, which were randomly assigned to different treatment groups (Tumor-control, TMZ-treated, FU-treated, and TMZ+FU-treated), with 6 animals in each group. Post treatment, the survival of the experimental groups was observed every day and recorded for a period of 175 days to plot Kaplan-Meier survival curve. Death of each animal is measured by the number of break points in an experimental group. Rats surviving beyond 175 days, were euthanized according to the ethical guidelines.

5.18 Toxicity studies

Additionally, to assess if any toxicity was induced by the drugs, post-cervical dislocation was performed to remove the vital organs, such as heart, lungs, liver, pancreas, spleen and kidney by a mid-line incision in the abdomen. These organs were formalin-fixed, embedded in paraffin, sectioned, and subjected to histopathological evaluation. Images were captured at 40x magnification and quantified using ImageJ software.

5.19 Detection of Ultrastructural changes by Scanning Electron Microscopy (SEM)

To substantiate the efficacy of the dual-drug combination at ultra-structural and morphological levels induced by the drugs, both individual and in combination, Scanning Electron Microscopy (SEM) was performed. Rat brain tissues were sectioned using an ultramicrotome, and gently compressed in 8 mm square-shaped cover slip and fixation was followed according to the protocol described by Campora *et al*. 1978 (61). Quantification of SEM images in terms of the number and size of grooves was performed by ImageJ.

5.20 Immunohistochemistry Analysis

To elucidate the underlying pathological effects at molecular levels, immunohistochemistry (IHC) analysis was performed against each of the experimental groups. For this purpose, tissue sections from each experimental group were formalin-fixed and sectioned (5 µm). Following deparaffinization, antigen retrieval was performed by heating the formalin-fixed sections in a microwave for 20 minutes in sodium citrate buffer containing 10 mM sodium citrate and 0.05% Tween-20 (pH 6.0). Endogenous peroxidase activity was blocked by incubating the tissues in 3% H_2O_2 for 15 minutes. The tissue sections were then blocked with 3% bovine serum albumin (BSA) for 10 minutes. After washing in 1X-TBST buffer twice, the slides were sequentially incubated with primary antibodies (rabbit anti-TLR4 antibody

1:100 dilution; rabbit anti-IL6 antibody 1:100 dilution; rabbit anti-JAK2 antibody 1:100 dilution, rabbit anti-STAT3 antibody 1:50 dilution, rabbit anti- NOS2 1:50 dilution and rabbit anti-IFN-γ antibody 1:30 dilution) for 1 hour at room temperature. After washing off unbound antibodies, HRP-conjugated secondary antibody incubation for each of the sections was executed for 30 minutes at room temperature. The bound antibodies were detected using diaminobenzidine (DAB), counterstained with hematoxylin, and mounted using a mounting medium (Dako, Denmark). Microscopic images were obtained using an inverted microscope (Primo Star, Carl Zeiss, Germany). Positive expression of each of these molecules has been interpreted in terms of immunoreactive scores (IRS) as listed in Table 6.

5.21 STATISTICAL ANALYSIS

All of the experiments were performed in triplicates and represented as mean ± standard deviation (SD). Analysis of the experimental data was carried out using GraphPad Prism v.8.0.1 (GraphPad Software, San Diego, CA, USA). Statistical analysis between the control and various experimental groups was performed using Analysis of Variance (ANOVA). Post-hoc analysis was carried out using Dunnett or Tukey's post-hoc test. $P< 0.05$ was considered to be significant.

6.0 RESULTS

Cytotoxic effects of TMZ and FU on glioma cells

To validate the cytotoxic effect of the drugs, both individually and in combination on glioma cells, MTT assay was performed wherein; the cells were treated individually with varying concentrations of the drugs namely 10, 50, 100, 150, 200, 250, and 300 µM. In the present study, both the chosen drugs (TMZ and FU) had depicted a significant anti-proliferative effect against glioma cells. Among the two drugs employed for the current study, individually, TMZ had displayed a prominent growth inhibitory effect in dose-dependent fashion (IC_{50}: 50 ± 0.003 µM). However, FU as an individual drug showed only a moderate cytotoxic effect as evident from its IC_{50} value (150 µM± 0.02 µM) (Figure 4A).

Having determined the individual IC_{50} values of the drugs, we then assessed the effect of the combinatorial treatment on glioma cells. For this, the IC_{20} of TMZ (identified to be more potent based on individual IC_{50} values) was kept constant and the concentration of FU was varied. Post 24 hours of treatment, we observed that the exposure to combinatorial treatment had sensitized glioma cells more significantly ($p<0.05$) than the effect observed in mono-therapeutic regimes.

To note, when administered as a combinatorial treatment, the concentration of TMZ and FU was reduced to 1.2µM and 89.04 µM respectively (Figure 4A). This data highlights the fact that FU can elevate the sensitivity of the cells to TMZ, at a minimal dosage. After 24 hours of treatment, the IC_{50} values of TMZ-alone, FU-alone and TMZ+FU in C6 glioma cells were found to be 50 ± 0.003 µM,150 ± 0.02 µM and 89.04 ± 0.05 µM respectively (Figure 4A).

Further, in order to determine whether the individual and dual-drug treatment of TMZ and FU were toxic to normal cells, cytotoxicity was evaluated on HEK293T normal transformed cell line. We observed that the IC_{50} values obtained for individual and dual-drug treatment (TMZ+FU) on HEK293T were higher than that of glioma cells. These findings suggest that individual and combinatorial treatment of TMZ+FU was found to be more cytotoxic and sensitive to glioma cells, rather than the normal cells (Figure 4B).

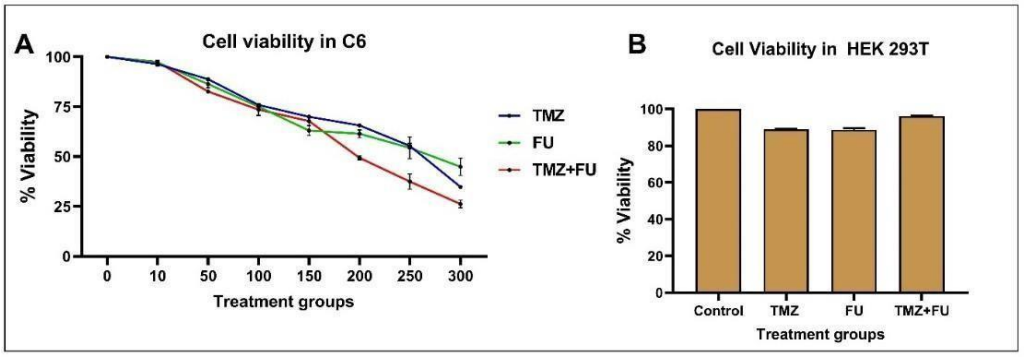

Figure 4: Cytotoxicity analysis of TMZ and FU, individually and in combination on (A) C6 and (B) HEK293T cells. Data points represent mean ± SD from triplicate.

Selectivity index (SI)

Selectivity index (SI) of TMZ, FU and their combination of TMZ+FU were evaluated from the cytotoxicity assay performed on C6 and HEK293T cells. Drugs possessing higher SI values are considered to be more efficacious against cancer cell lines at concentrations obtained below the cytotoxic concentration of normal cells. The SI values from the present study revealed that the IC_{50} of TMZ in HEK293T cells was 5-fold greater than in C6 and IC_{50} of FU in HEK293T was 2-fold greater than in C6 cells, whereas combination of TMZ and FU showed a fold change of 2.24 greater in HEK293T, than that of C6 cells (Table 3).

Table 3: Selectivity index (SI) analysis

Drugs used	IC50 value in C6 glioma (µM)	IC50 value in HEK293T cells (µM)	Selectivity Index (SI)
TMZ	50	250	5
FU	150	300	2
TMZ +FU	89.04	200	2.24

Synergistic effects of TMZ and FU on glioma cell proliferation

To determine whether the cytotoxic effects of the dual-drug combination (TMZ+FU) were additive, synergistic or antagonistic, normalized isobologram and statistical combination index (SCI) for non-constant ratio combination design was assessed. CI values were calculated by the Compusyn software according to the recommendations of Chou-Talalay, wherein combinatorial drug treatment (TMZ+FU) exhibited strong synergistic effect at an IC_{50} value of 89.04 µM (Figure 4A and 5A), CI index of 0.62 (Figure 5B). Besides, DRI value of the dual-drug combination was obtained more than 1, at its IC_{50} value, suggesting a favourable synergism (Figure 5C). These results suggest that the combinatorial-drug treatment of TMZ and FU, exhibited maximum synergistic cytotoxicity against glioma cells.

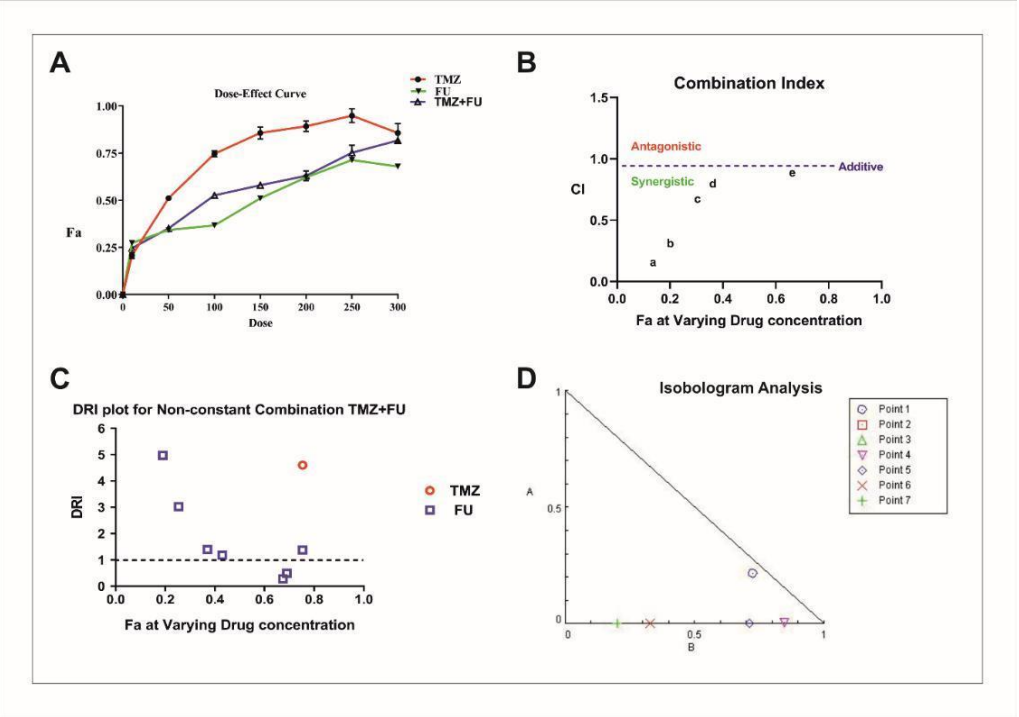

Figure 5: Combination Index Analysis using Compusyn (A) Dose-effect curves for TMZ, FU and TMZ+FU after 24 hours of treatment
(B) Combination index plot: The combination index is plotted as a function of Fa (C) Dose reduction index plot for combination: Dose reduction index values at different Fa values for each drug in the combination (D) Isobologram

analysis: Combination index determined with respect to different drug dosages (A-TMZ and B-FU), and the points represent the CI values obtained below 1.

One of the major hallmark for glioma pathogenesis is migration, which is a key contributing factor for most of the treatment failures (62). Inhibition of glioma proliferation of the combinatorial treatment drove us to investigate if this dual-drug cocktail could also hamper glioma migration. Thus, we performed wound healing assay and measured the cell-free area at 0 and 24 hours, following exposure to the drugs. Though the efficacy of TMZ (Figure 6F) and FU (Figure 6G) as individual drugs was relatively modest on sustaining the cell-free area, the combinatorial treatment (TMZ+FU) had rarely promoted the migration of glioma cells, with the cell-free area of micro-metre (µM). This highlights the fact that the combinatorial treatment (TMZ+FU) besides exhibiting significant anti-proliferative effect, can also inhibit the mobility of glioma cells (Figure 6H).

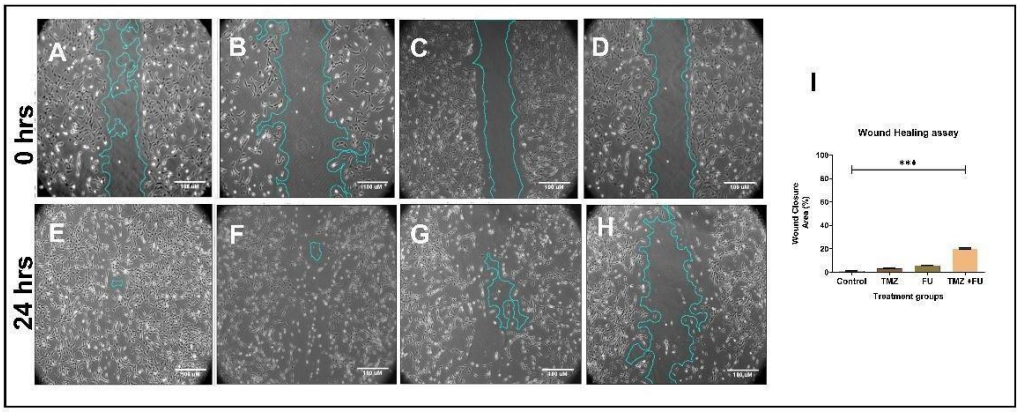

Figure 6: Inhibition of cell migration under the different treatment groups for (A & E) Control, (B & F) TMZ, (C & G) FU and (D & H) TMZ + FU after 24 hrs. (I) Percentage of cell migration was calculated on the width of remaining wound surface area relative to the initial wound surface area. *** indicates $p \leq 0.001$, compared with control.

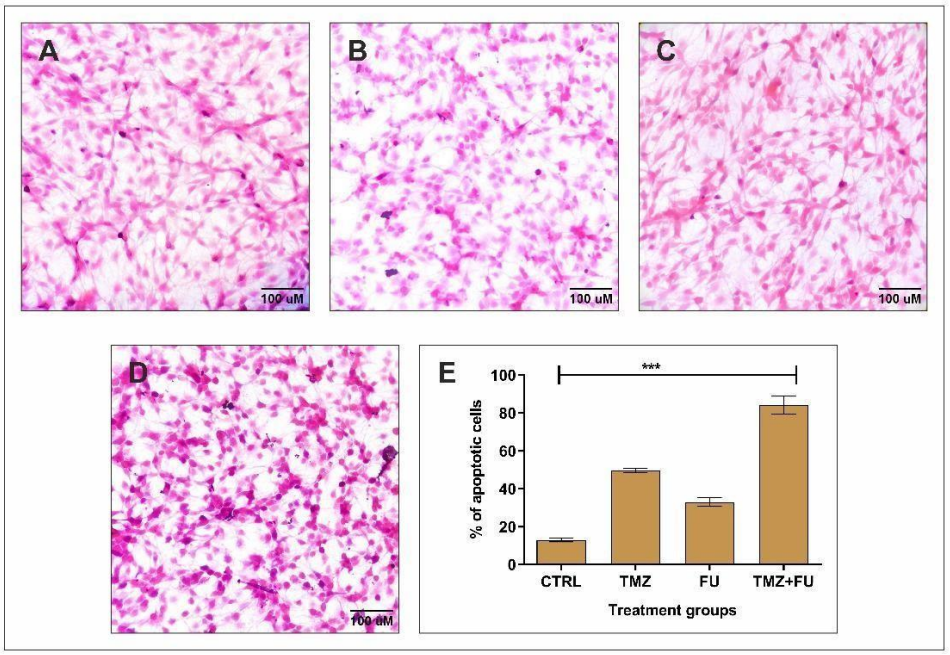

Figure 7: Apoptotic cell death observed using Hematoxylin and Eosin (H & E) stain under different treatment groups on C6 glioma cells (A) Control, (B) TMZ, (C) FU, (D) TMZ+FU and (E) Percentage of cells was calculated as total cellular shrinkage and loss of integrated density. *** indicates $p<0.001$, compared with control.

Combinatorial Effects of TMZ and FU on apoptosis in C6 glioma cells

With the aim of understanding the inhibitory mechanism elicited by TMZ, FU or their combination on glioma cells, we analyzed the induction of apoptosis at morphological level by few staining procedures. This is due to the fact that, evasion of apoptosis is a distinct feature of most of the cancer cells including glioma (63).

Firstly, we performed H&E staining, wherein we found that treatment with TMZ-alone had endowed moderate rate of apoptosis (49.6%, Figure 7A) with shrinking nuclei and the cells had very poor demarcation of the nucleus and cytoplasm, when compared with that of control (untreated) cells. FU treatment on the other hand, resulted only a few number apoptotic cells (Figure 7B), while most of the cells had a clear cytoplasm and nucleus, denoting that FU as an individual drug had moderate apoptosis induction potency but was not as effective as the standard drug, TMZ (33.06%). Interestingly, cell which were exposed to the combinatorial treatment (TMZ+FU) portrayed a large number of apoptotic cells (84.11%) with cell shrinkage (Figure 7D), and their viability was drastically reduced. Also, the cells had displayed marginated, condensed and aggregated nuclei,

which all are the morphological characteristics of apoptosis.

Following affirmation that the combinatorial treatment restrained glioma growth and induced apoptosis by H&E, we were also interested to distinguish the cells at different stages of apoptosis following administration of these drugs. For this purpose, AO/EtBr stain was employed. AO penetrates the live cells or cells in the early stage of apoptosis and stains them yellow-green, while EtBr is only permeable to the late-apoptotic cells with compromised cell membrane, emitting orange-red fluorescence. In accordance with this principle, our staining results revealed that in individually TMZ-treated cells (Figure 8B), a large number of cells at the early apoptotic stage (24%), and emitting yellow-green fluorescence was observed. On the other hand, treatment with FU (Figure 8C) also resulted in a large number of early apoptotic cells and few late apoptotic cells (32.3%), signifying the early apoptotic effect of FU. Interestingly, combined administration of these drugs as a dual-drug treatment resulted in a large number of late-apoptotic cells (45%), emitting orange-red fluorescence (Figure 8D). Also, a small proportion of the cells displayed an uneven orange-red fluorescence pattern, with increased cell volume, thereby denoting that the cells had undergone necrosis.

Following the analysis of cytoplasmic changes induced by the combinatorial treatment via H&E and AO/EtBr stains, we then employed the nuclear stain, DAPI to evaluate the alterations induced by TMZ, FU and their combination at nuclear level. Following staining, cells assigned as control, depicted a clear and distinct nucleus. As expected, the nuclear morphology in the treated cells was altered in all the treatment groups employed for our study. Among the individual drugs, treatment with TMZ endowed 70.48 % of apoptotic cells with condensed and marginated nuclei (Figure 9B). However, treatment with FU resulted only in 67.28% of apoptotic cells (Figure 9C) with condensed nuclei. The most significant nuclear alterations were apparent in the combinatorial treatment (TMZ+FU), wherein 73.3% of apoptotic cells with highly shrinked nuclei and patterns of nuclear fragmentation were observed (Figure 9D). Taken together, our staining results suggested that the combinatorial treatment was bestowed with the potency to induce apoptosis at both cytoplasmic and nuclear level, besides suppressing glioma proliferation and migration.

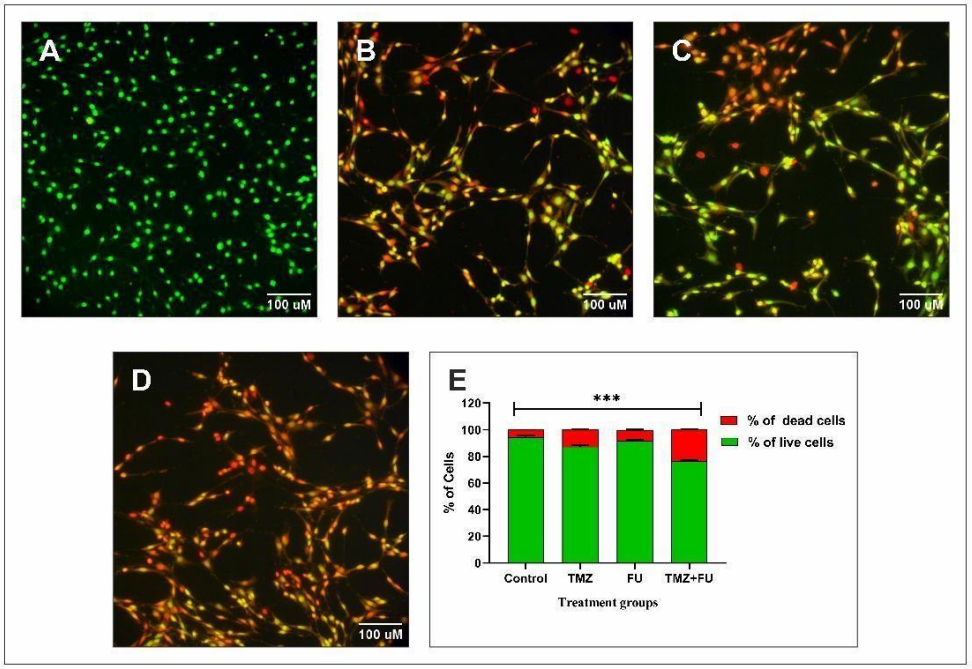

Figure 8: Apoptotic cell death was observed by AO/EtBr staining under different experimental treatment groups on C6 glioma cells-(A) Control, (B) TMZ (C) FU (D) TMZ+ FU, (E) Percentage of apoptotic cells were measured by scoring viable and dead cells. *** indicates $p<0.001$ in comparison to untreated control.

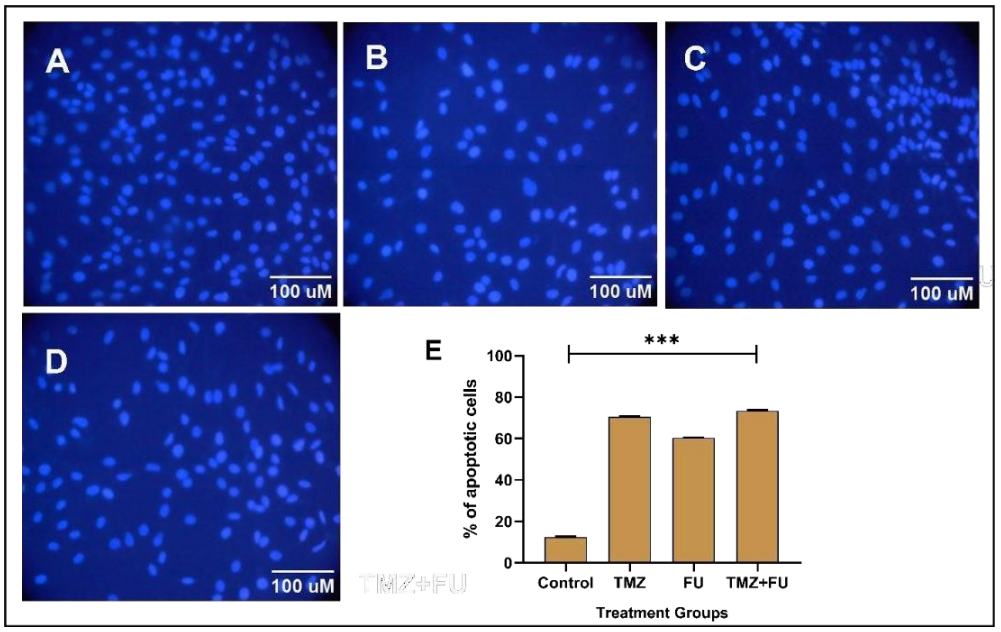

Figure 9: DAPI staining under different experimental treatment groups on C6 glioma cells- (A) Control, (B) TMZ (C) FU (D) TMZ+FU, *** indicates $p<0.001$ in comparison to untreated control.

Dual-drug combination modulated the gene expression levels of inflammatory and pro-apoptotic markers in C6 glioma cells

Observations from the staining techniques led us to investigate the underlying molecular mechanism of this combinatorial treatment on glioma cells. Hence, we analysed the relative mRNA expression levels of inflammatory and pro- apoptotic genes namely IL-6, TLR-4, MYD88, IFN-γ, STAT3, NOS-2 and caspase-3 by qRT-PCR analysis. It is worth noting that the inflammatory genes IL-6, TLR-4, MYD88, NOS2, STAT3 and IFN-γ were aberrantly expressed in glioma's and may contribute to tumor progression and chemo-resistance (64). Treatment with TMZ and FU, as individual drugs, had significantly down-regulated the expression levels of the inflammatory genes while concomitantly increasing the mRNA expression of caspase-3 to a considerable extent (Figure 10). Interestingly, among all of the experimental groups, the combinatorial treatment of TMZ+FU displayed a significant decrease in the fold change of inflammatory genes while up-regulating the fold change of caspase-3, thereby denoting that this combination elicited apoptosis by down-regulating the inflammatory signaling cascade (Figure 10).

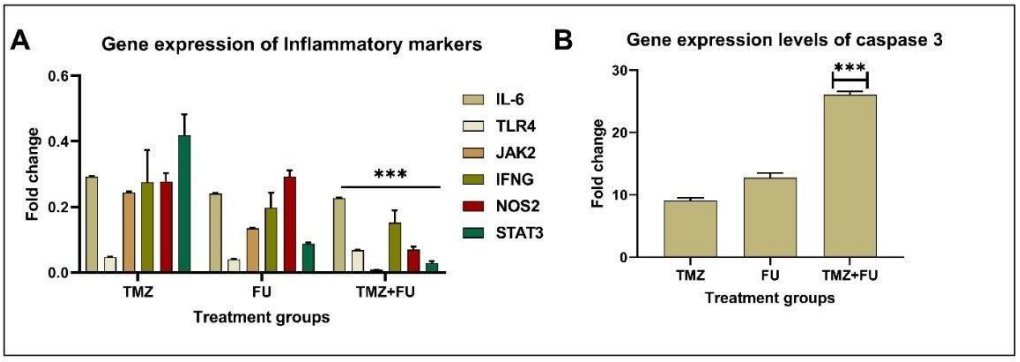

Figure 10: Anti-glioma effects of FU, both alone and in combination with TMZ on the mean fold change (Linear scale) of inflammatory genes (A) IL-6, TLR4, MYD88, IFN-γ, NOS2, STAT3 and (B) apoptotic gene-caspase-3 in C6 glioma cells. *** indicates $p<0.001$ in comparison to untreated control.

Molecular docking

Active site prediction

The active sites were predicted using Sitemap prediction tool (Schrodinger) and has been listed below in the Table 4.

Table 4: List of active site residues for each of the inflammatory targets

Sl. No.	Protein Targets	Residues involved in active site
1.	IL-6	Ile72, Arg74, Leu89, Leu90,Lys91,Ile92,Phe179,Thr183,Ser 186
2.	TLR4	Arg233, Phe262, Lys263, Asp264, Tyr291, Ala314, Gly315, Arg337
3.	JAK2	Leu824, Val832, Ala849, Val880, Met898, Glu899, Tyr900, Leu901, Pro902, Glu904, Leu952
4.	STAT3B	Trp243, Lys244, Gln247, Val322, Val323, Glu324, Gln326, Thr456, His457, Pro487
5.	IFN-γ	Gln1, Met45, Gln46, Ser47, Phe60, Thr96, Asn97, Tyr98, Ser99, Val100
6.	NOS2	Thr184, Trp188, Ala191, Cys194, Leu203, Ala237, Ile238, Phe363, Asn364, Tyr483.

Molecular Docking analysis

In order to predict the interaction of the ligands with the key drivers of inflammation in glioma, docking analysis was performed for the following targets namely, IL-6, TLR4, JAK2, STAT3B, IFN-γ and NOS2. The detailed interaction profile of the ligands with inflammatory proteins has been tabulated in Table 5.

Interestingly, we found that, all of the anti-tumor ligands viz., TMZ, MTIC, AIC and FU interacted with IL-6 by H-bonds predominantly. With regard to the binding energies, we observed that, TMZ, MTIC and AIC formed more number of H-bonds and exerted a binding energy of -23.953, -13.480 and

-28.148 Kcal/mole (Table 5). Although FU exhibited only two H-bonds with IL-6 (Figure 11) depicted a highest binding energy of -28.902 Kcal/mole (Table 5). This could be due to the presence of other non-bonding interactions, which could have facilitated the stronger interaction of FU with IL-6 (Figure 11). In the case of TLR4, we observed that TMZ, MTIC, AIC and FU interacted through H-bonds and salt bridge formation (Figure 11), with a binding energy of -27.448, -40.175, -25.524, and -23.074 Kcal/mole, respectively (Table 5). Among the anti-tumor ligands, MTIC, despite possessing lesser number of H- bonds and salt bridges, depicted the highest binding energy (Figure 11).

A similar pattern of interaction was observed in the case of JAK2, whereby, MTIC exhibited the highest binding energy of -42.885 Kcal/mole, while the remaining ligands- TMZ, AIC and FU exerted a binding energy of -32.530, -33.159 and -29.593 Kcal/mole, respectively (Figure 11, Table 5).

Likewise, the docking analysis for STAT3B, revealed that, MTIC depicted the highest binding energy of -28.236 Kcal/mole, while TMZ, AIC and FU exhibited binding energy of, -20.667, 17.346 and -23.658 Kcal/mole respectively (Figure 12, Table 5). The binding energy of MTIC could be due to the formation of π-cationic interaction along with H-bond that contributed to the overall stability, when compared with the other anti-tumor ligands (Figure 12). In the case of IFN-γ, docking results revealed that AIC depicted the maximum interaction profile with a binding energy of -36.282 Kcal/mole (Figure 12), while TMZ, MTIC and FU exerted a binding energy of -31.600, -24.403 and - 23.932 Kcal/mole respectively (Figure 12, and Table 5).

With the most crucial target, NOS2, docking analysis revealed that AIC exhibited a highest binding energy of -33.902 Kcal/mole (Figure 12), following, FU, TMZ and MTIC of -24.978, -24.211 and -20.902 Kcal/mole (Figure 12). This accounts for the presence of maximal number of H-bonds and salt bridge formation, as compared to other ligands and hence the maximum stability (Table 5).

To summarize, the complexity of bonding between the ligand-target protein complexes denotes the strength of molecular docking. From our visual analysis,

based on the binding energy and docking score, it was evident that TMZ and its metabolites, MTIC and AIC were the best ligands to form complexes with TLR4, JAK2, STAT3B, IFN-γ and NOS2, while FU exhibited highest interaction with IL-6. However, further investigations were warranted for verification of the stability of these ligand-protein complexes obtained by docking analysis.

Table 5: Interaction profile of all the inflammatory targets against the four ligands

Ligands	**Interaction type**	**Functional moieties {} - Interactions with same amino acid residues**	**Amino acid residues**	**Binding Energy (Kcal/mole)**
IL-6				
TMZ	H-bonds (4) /salt bridge (1)	NH_2 (at 1 position of tetrazine ring), NH (6^{th} position of tetrazine ring), O^- (7^{th} position) of carboxamide) and NH_3^+ (8^{th} position) of carboxamide in imidazole ring/	Leu90, Leu89, Ile87, Ser186/ Lys91	-23.953
MTIC	H-bonds (3)	NH_2^+ (1^{st} position), N^+H_2 (3^{rd} position), O^- (4^{th} position) of carboxamide and NH_2 (5^{th}) position of tetrazine ring	Lys91, Leu90, Arg74	-13.480
AIC	H-bonds (4)	OH (at 1^{st} position), NH_2^+ (2^{nd} position), {NH_2^+ (4^{th} position), substituted chain (at 5^{th} position,	Gly77, Cy78 and Gln85,	-28.148

		NH-3rd position)} of imidazole ring		
FU	H-bonds (2)	OH (4-Hydroxy), O—SO_3 (at 5th position) (sulphate) of Fucose ring /	Leu89, Leu90	-28.902
TLR4				
TMZ	H-bonds (3)/ salt bridge (3)	{NH^+ at 4th position and N^+H_2at 6th position, N^+H_3 at 8th position} of imidazole ring/ {NH^+ at 4th position and {N^+H_2 at 6th position}, N^+H_3 at 8th position}} of Imidazole ring	Asp 208, Glu229/ Asp180, Asp208 and Glu229	-27.448
MTIC	H-bonds (3) /salt bridge (2)	NH_2^+ (at 1st position), {NH_2^+ (at 3rd position), NH_3^+ (at 4th position-of imidazolidin)}/ NH_2^+ (at 1st position), NH_2^+ (at 3rd position) of imidazole ring	Glu229, Asp208/ Glu229 and Asp208	-40.175
AIC	H-bonds (5) /salt bridge (3)	N^+H_3 (1st), NH_2^+ (2nd), NH_2^+ (4th), 5th-substituted chain (1st and 3rd NH-NH) of imidazole ring/ NH_2^+ (2nd) of imidazole ring	Glu229, Asp208 / Glu229, Asp180, Asp 208	-25.524

FU	H-bonds (2) /salt bridge (1)	O-$SO3^-$ (at 3rd position) and OH (5-hydroxy) of Fucose ring	Arg233, Arg337/ Lys263	-23.074
JAK2				
TMZ	H-bonds (3)/ salt bridge (2)	O^-(4th position) of carboxamide, NH_2^+ at 7th and 8th position of imidazole ring – (OH & NH_2)/ O^-(4th position) of carboxamide and NH_2^+ at 7th position of imidazole ring	Leu824, Cys905, Asp 908, Asp908/ Arg912 and Asp908	-32.530
MTIC	H-bonds (7)	N^+H_2 (at 1st position), N^+H_2 (3rd position), OH & NH_2 (at 4th position) of imidazole ring	Tyr900, Ser 573, Leu583, His510, Tyr900 and Pro902	-42.885
AIC	H-bonds (7)/ salt bridge (1)	NH_2 and OH (1st position), NH and NH_2^+ (2-(3-methyl- 2λ4-triazenyl), NH (3rd position) and NH_2^+ (5th position) of imidazole ring/ NH_2^+ (5th position) of imidazole ring	Asp963, Arg949, Asn826, Leu824/ Asp963	-33.159
FU	H-bonds (4)	O-SO_3^- (3rd) of sulphate, OH at 4th and 5th position of Fucose ring	His510, Arg912, Ser903, Pro902	-29.593

STAT3B				
TMZ	H-bonds (3)/ salt bridge (1)	NH (at 1st position), NH_3^+ (at 9th position), of imidazole ring/ O^- at 3rd position (oxidanyl group) of imidazole ring	Glu455, His457/ Lys244	-17.346
MTIC	H-bonds (4)/ pi (π)-cation (1)	{NH_2 (at 1st position), NH_2} (2nd position at imidazolidin-4-yl), NH (5th position)/ NH_2^+ (at 3rd position) of imidazole ring	Gln247, Val323 and His457/His457	-28.236
AIC	H-bonds (4)/ salt bridge (2)/ pi (π)-cation (1)	NH_3^+ (at 1st position), {NH_2^+ (4th position), substituted chain (5th position of 1st and 3rd NH-NH)} of imidazole ring /NH_2^+ at 2nd position of imidazole ring/ NH_2^+(2nd position of substituted chain)	Glu455, Asp371/ Glu455, Asp371/ His457	-20.667
FU	H-bonds (2)	OH at 3rd position and O-$SO3^-$ (at 5th position) of Fucose ring	Thr456, His457	-23.658
IFN-γ				
TMZ	H-bonds (4)	NH (at 7th position), OH & NH_2 (at 9th position) of imidazole ring	Cys178, Glu175, Thr172	-31.600
MTIC	H-bonds (3)	{NH (4th position), (carboxamide), NH_3^+ (5th position)}, of imidazole ring	Cys178, Thr172 and Thr172	-24.403

AIC	H-bonds (7)/ salt bridge (1)	NH (at 1st position), NH-NH (at 1st and 3rd position), NH_3^+(3rd position), NH_2^+(4th position) of imidazole ring/ NH_2^+(4th position) of imidazole ring	Cys178, Asp176, Asp176, Glu175 and Gln173	-36.282
FU	H-bonds (3)	OH (3,4-dihydroxy), $O=SO_3^-$ of Fucose ring	Phe134, Ile152	-23.932
NOS2				
TMZ	H-bonds (2)/ pi (π)-cation (2)	{NH_2 and OH} (at 8th position)/NH_2^+ at 7th position of imidazole ring	Asn364, Phe363 and Trp188	-24.211
MTIC	H-bond (1)/ pi (π)-cation (2)	NH_2 (at 2nd position)/ NH_2^+ (4th position) and C-at 5th position of imidazole ring	Asn364/ Trp188 and Phe363	-20.902
AIC	H-bonds (6)/ salt bridge (1)	{NH_2 (at 1st position), (1st and 3rd position NH-NH at 2nd position of substituted chain,), {N^+H_2 (3rd position), N^+H_2 (5th position) and OH (1st)} of imidazole ring/ N^+H_2 (3rd position) of imidazole ring	Trp366, Glu361/ Glu361	-33.902
FU	H-bond (1)	O^--SO_3 bonded at 2nd position of Fucose ring	Tyr485	-24.978

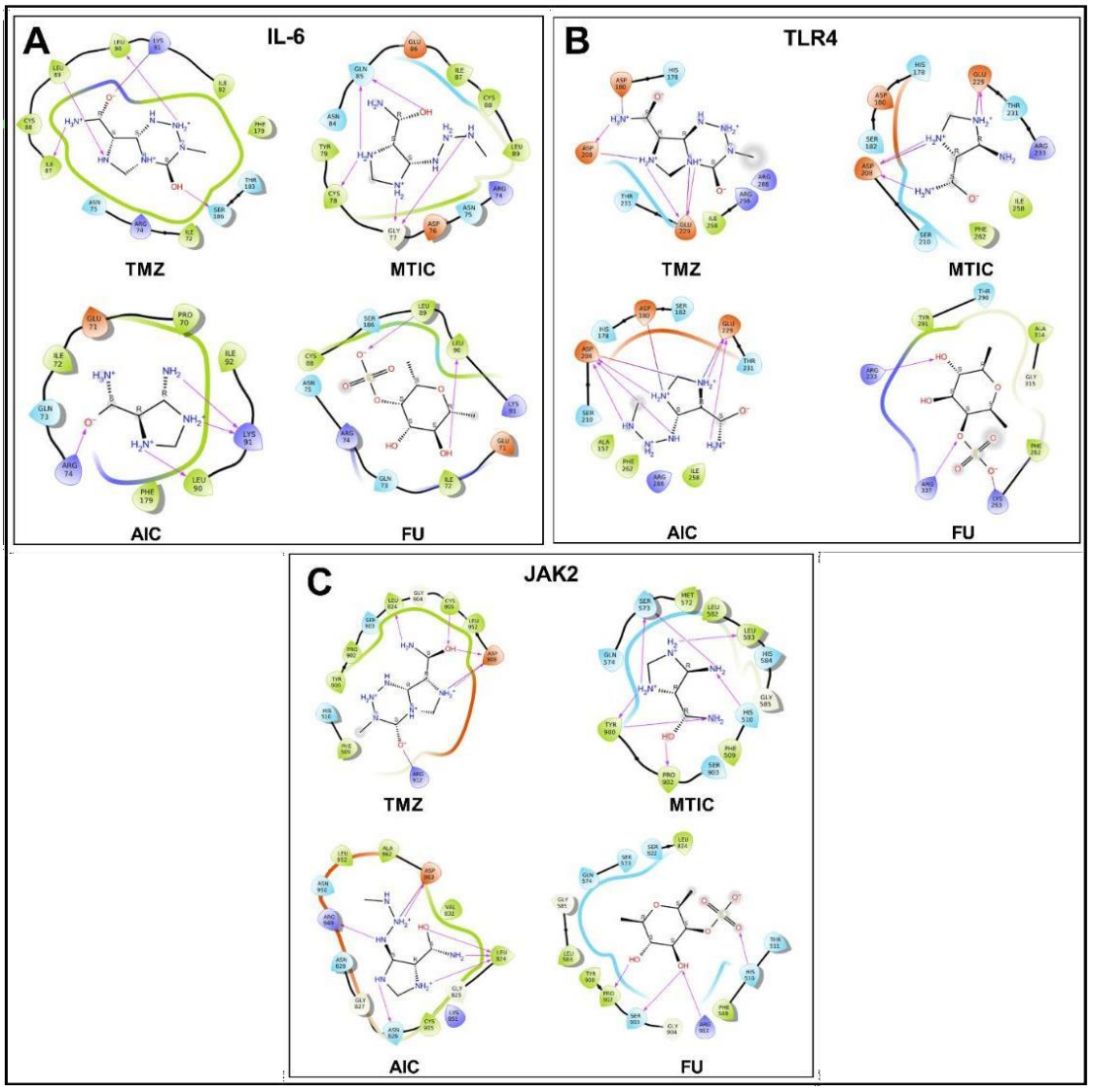

Figure 11: Interaction profile of (A) IL-6, (B) TLR4, (C) JAK2 with ligands- TMZ, MTIC, AIC and FU

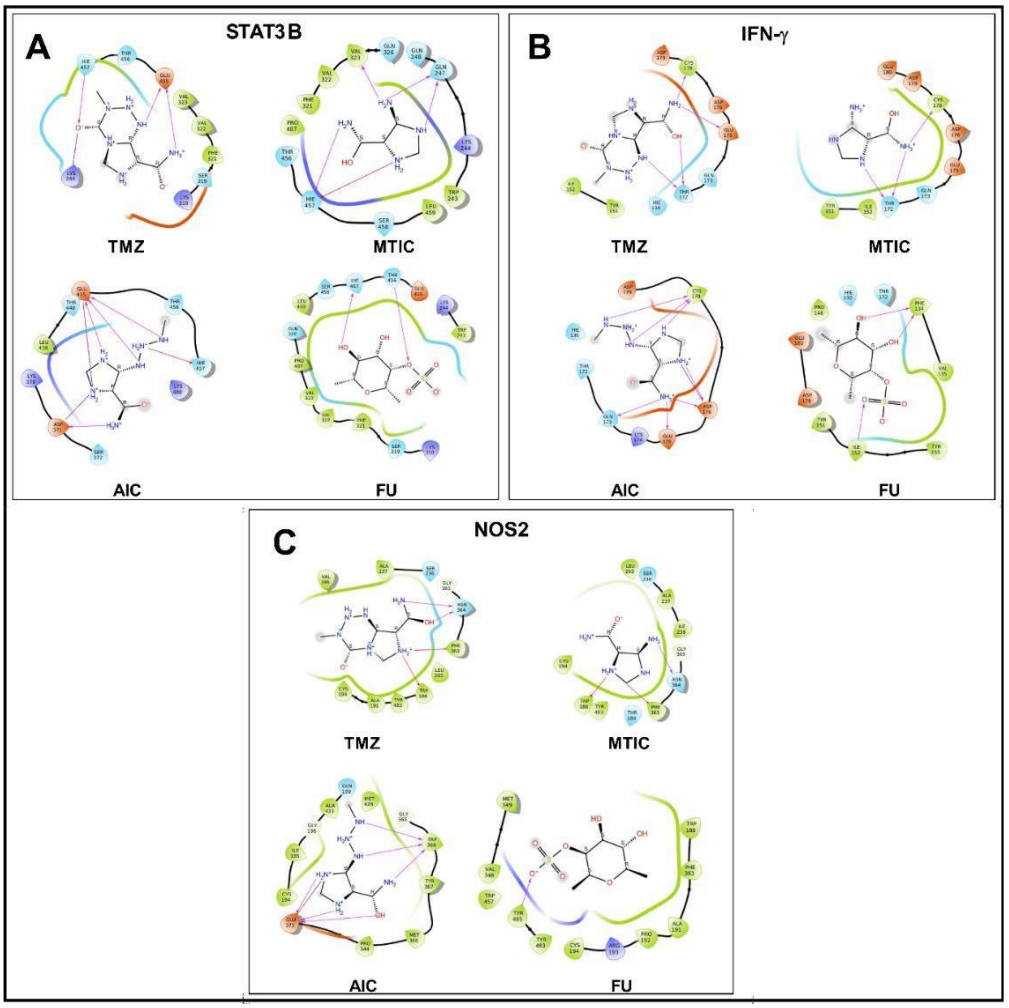

Figure 12 : Interaction profile of (A) STAT3B, (B) IFN-γ and (C) NOS2 with ligands TMZ, MTIC, AIC and FU

Molecular dynamics simulation (MDS)

Following identification of the docked complexes and affirmation of their interaction profile, we then determined the stability of these interactions using Molecular Dynamics Simulation (MDS). MDS was evaluated in terms of RMSD, RMSF, Rg and SASA against each of the docking complexes. Among the MDS parameters, RMSD is used to measure the average change in displacement of atoms of a particular frame with respect to a reference frame. In general, the target reaches stability in few pico-seconds (ps). Initially RMSD was performed for IL-6 whereby we found that, TMZ, MTIC and AIC depicted a stable interaction (0.5-0.59 nm) with the target protein till 20000 ps, while FU exhibited a slight increase in the RMSD value (0.66 nm) from 15000 ps (Figure 13). Similar to their interaction with IL-6, the ligands TMZ, MTIC and AIC showed a rise from (0.6-0.9 nm), following consistent RMSD plot (0.9 nm) for TLR4 as well, while FU portrayed a mild increase in RMSD value (1.2 nm) from 10000 ps. Interestingly, all of the four ligands displayed an overall stability for JAK2 and STAT3B at 20000 ps (0.4 nm). On the other hand,

RMSD plots of IFN-γ and NOS2 revealed a stable RMSD value (0.2 nm) for all the chosen ligands, except AIC, which showed elevation in the RMSD plot (IFN-γ-0.8 nm at 15000 ps; NOS2- 0.6 nm at 10000 ps) (Figure 13). Based on the RMSD studies, we concluded that all of the chosen protein-ligand complexes had attained structural stability against all of these docked complexes.

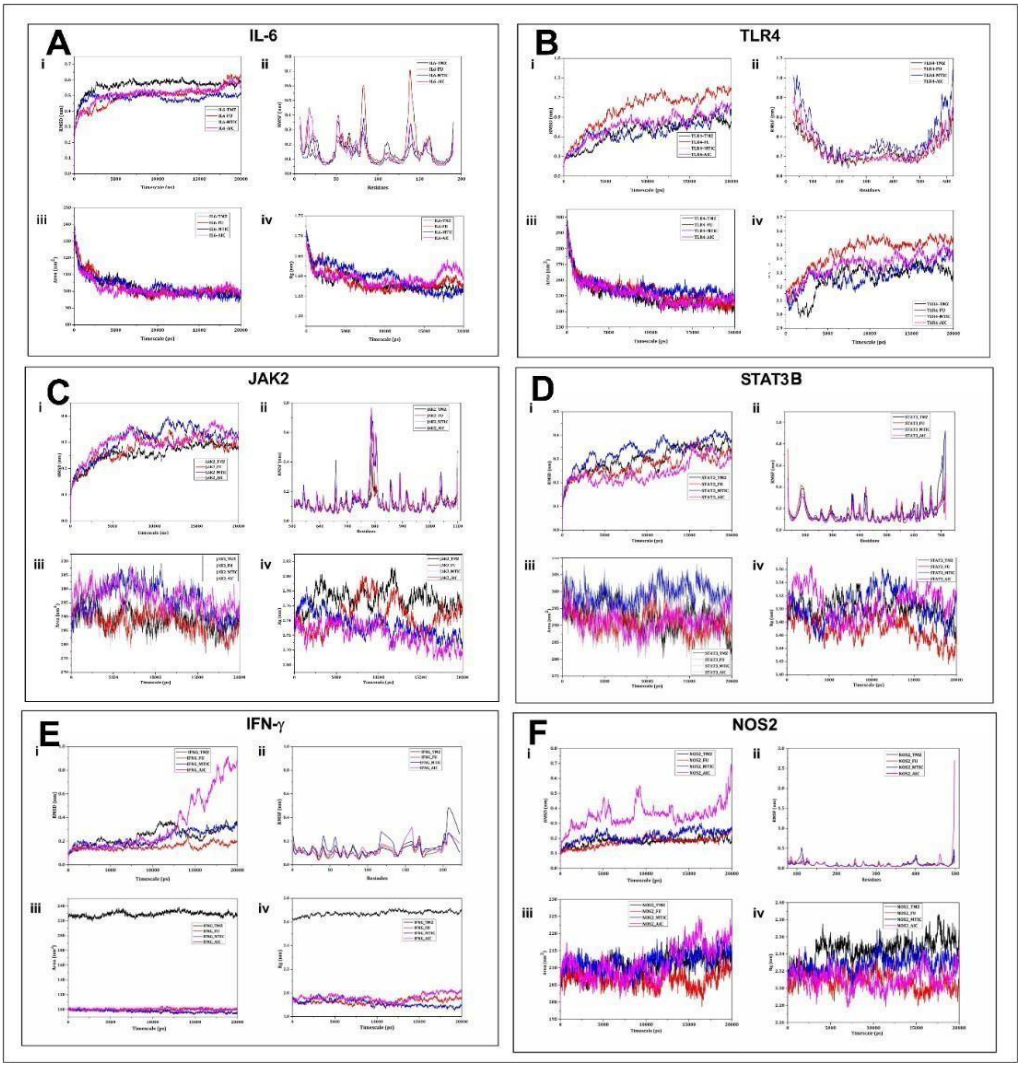

Figure 13: RMSD, RMSF, Rg and SASA plots for (A) IL-6, (B) TLR4, (C) JAK2, (D) STAT3B, (E) IFN-γ and (F) NOS2.

To further verify the ligand-protein stability, we then evaluated the RMSF value for the ligand-protein interactions. RMSF plot enables to predict if the ligand-target interaction is sufficiently stable and provides basis for the flexibility of the conformation. RMSF fluctuation is often connected to RMSD plot, wherein more RMSF fluctuation yields less stable RMSD plot.

Interestingly, we found that among the ligands that interacted with IL-6, TMZ, MTIC and AIC exhibited the minimum fluctuation (<0.4 nm) while FU depicted the maximum fluctuation (0.7 nm) (Figure 13). In the case of TLR4, RMSF plot revealed that among all of the four ligands interacted, TMZ, AIC and FU showed the minimum fluctuation (<0.8 nm) while MTIC exhibited maximum fluctuation of 1.0 nm. Conversely, the RMSF plots of JAK2 revealed minimal fluctuation in TMZ (0.4 nm) and maximum fluctuation for MTIC, AIC and FU (0.8 nm). On the other hand, amongst all of the docked complexes, MTIC, AIC and FU depicted a minimal fluctuation (<0.4 nm) with IFN-γ, while TMZ demonstrated a slight increase in RMSF (at 200 residues). With regard to their interaction with NOS2, TMZ, MTIC and FU exhibited a minimum fluctuation of <0.5 nm, while AIC showed the maximum fluctuation (2.5 nm). Taken together, in consensus with our RMSD results, the RMSF affirmed that the ligand-protein complexes were sufficiently stable and had low flexible conformation.

SASA is used to determine the surface area on a biomolecule that is accessible to solvent molecules. SASA plot denotes the ligand-protein interaction in the solvent. In general, low SASA value denotes that the target protein is less available for interaction with the solvent molecules like water; High SASA value on the other hand, implies that the target protein is widely accessible by the solvent molecules. Interestingly, the SASA plots of the interactions between all the four ligands and IL-6 revealed a low SASA value (100-140 nm^2). Likewise, interaction between the ligands and TLR4 depicted a SASA value of 240-299 nm^2. On the other hand, interaction of the anti-tumor ligands with JAK2, STAT3B and NOS2 exhibited a SASA value of 285-305 nm^2, 285-305 nm^2 and 205-225 nm^2, respectively. In the case of IFN-γ, MTIC, AIC and FU exhibited a low SASA value of 100 nm^2, while TMZ exhibited slightly higher SASA value of 220 nm^2. Taken together, our SASA analysis revealed that most of the chosen proteins depicted a low SASA score and had no folding effect on complex stability.

Following elucidation of complex stability and surface exposure, the intrinsic dynamics of ligand-protein complexes were calculated by performing Rg on the docked complexes. It is well known that an increase in Rg values implies a decrease in the protein compactness leading to increased flexibility and less stability. Low Rg values on the other hand, denote stability and protein compactness. The Rg plots of all the chosen ligand-protein complexes are depicted in Figure 13. It can be seen that the Rg value of all the chosen ligands with IL-6 was measured between 1.55-1.70 nm with less fluctuation. In the case of TLR4, TMZ, MTIC and AIC depicted moderate high fluctuation and high Rg value between 3-3.4 nm at 10000 ps while FU depicted high fluctuation of 3.5 nm at 10000 ps. For JAK2, MTIC and AIC depicted low fluctuation with Rg value ranging from 2.7 to 2.74 nm, while TMZ and FU

demonstrated a high fluctuation rate of 2.76- 2.8 nm. However, all of these four ligands depicted a high fluctuation and Rg value for STAT3B ranging from 3.42 to 3.54 nm. For IFN-γ, TMZ depicted the highest Rg value of 2.6 nm, while MTIC, AIC and FU showed Rg value below 2 nm with low fluctuation. Parallelly, for NOS2, all the four ligands exhibited a low fluctuation and Rg value from 2.3 to 2.36 nm. Thus, from our Rg scores, we concluded that the chosen ligand-protein complexes had depicted sufficient stability and compactness.

Overall, our *in silico* data strongly established the fact the chosen anti-tumor ligands had formed stable and compact docking complexes with the inflammatory proteins and may be probed further, to modulate the inflammatory pathway in experimental setup as an affirmation of our *in vitro* findings.

Elucidation of histopathological effects of the individual and dual-drug combination treated glioma xenografts

To determine the anti-glioma efficacy of TMZ and FU, both individually and in combination on orthotopic xenograft model, histopathological analysis was performed. It was observed that the brain tissues of the healthy control rats (Group I) depicted normal neuronal architecture (Figure 14-I a). On the other hand, tumor-control brain tissues depicted pleomorphic, vascularized cells with uniform dense cellularity. About 90% of cells in the tumor control group (Group II, Figure 14-I b) were found to be in the actively dividing state with interspaced pseudo-palisading necrotic sites. Also, the cells in the tumor control group were found to be collected densely around the blood vessels at infiltrative margins of the tumor (Figure 14-I b). Interestingly, administration of the dual-drug combination (TMZ+FU) depicted maximum reduction in tumor growth significantly ($p<0.001$) in comparison to individual and tumor control experimental groups. However, individually, both TMZ and FU had reduced the tumor growth and cellularity to 45% and 55% respectively (Figure 14-I c and d), yet they were not as significant as that of dual-drug treated rats. Furthermore, the morphology of the brain tissues in the dual-drug (TMZ+FU) treated rats resembled similar histopathological features to that of the healthy control group, with very less mitotic cells (25%, as similar to the control). These findings suggest that the dual-drug combination (TMZ+FU) had imposed significant histopathological changes and reduced the number of viable glioma cells in comparison to the tumor-control and individual treatment groups (Figure 14-I d and II).

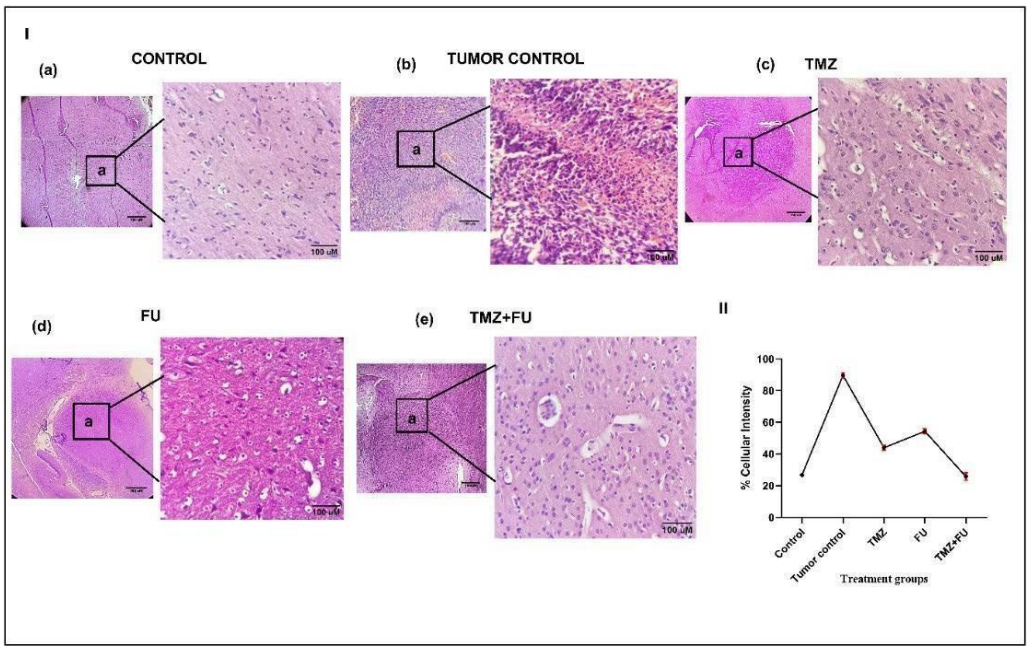

Figure 14: I-Histopathological analysis of the individual and dual-drug combination on glioma implanted brain tissues identified at 4X, wherein "**a"** denotes the actively dividing state of tumor growth against each of the experimental groups and under 40x magnification by inverted microscope (II)-Percentage cellular intensities (% cellular intensities) against each of the experimental groups, wherein dual-drug cocktail (TMZ+FU) depicted significant reduction, when compared with tumor-control and individual treatment groups ($p<0.0001$).

Assessment of the survival rate of glioma xenografts under the individual and dual-drug combination treatment

Following histopathological analysis induced by the individual and dual-drug treated drugs, the efficacy of this dual-drug combination on the overall survival of glioma-induced and drug-treated glioma xenografts was evaluated, by a 25-week follow-up study. From the Kaplan-Meier plot, it was observed that rats in the tumor-control (Group II) group began to die on the 5th week and all rats were dead by 8th week (56 days, Figure 15). Interestingly, administration of dual-drug combination did not exert any adverse effects and significantly enhanced the overall survival; wherein, the dual-drug combination treated rats began to die only on 23rd week (161 days) and all rats were sacrificed by 25 weeks (175 days) and the overall survival rate for TMZ and FU-treated rats were 105 & 70 days, respectively. Thus our survival analysis depicted that, the dual-drug combination of TMZ+FU (Figure 15) exerted maximal progression-free survival of the glioma-induced rats in comparison to individual and tumor-control groups.

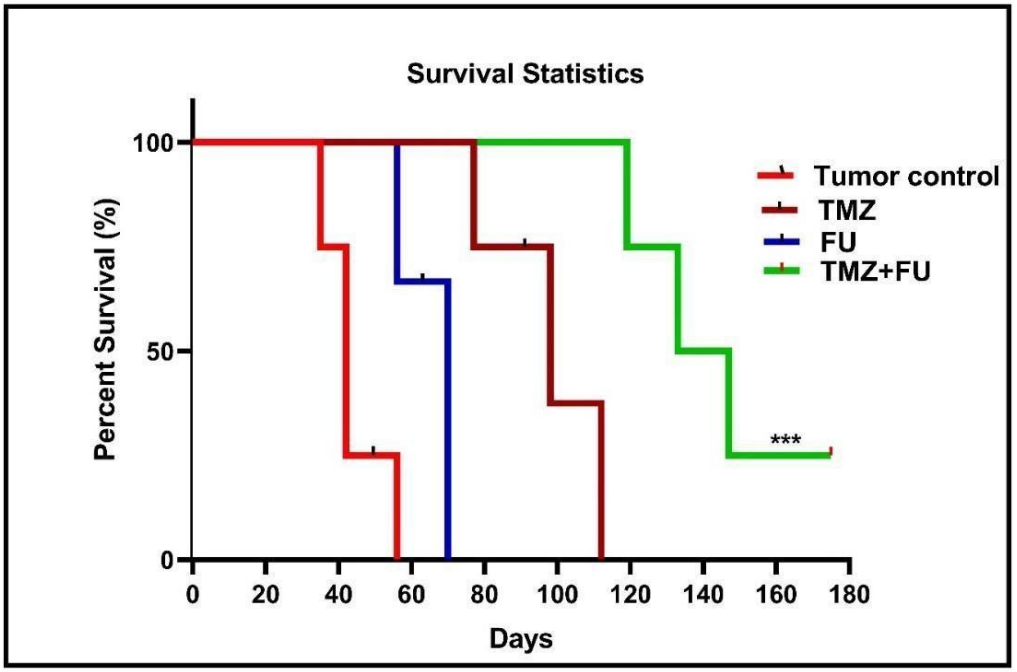

Figure 15: Kaplan-Meier survival curve of orthotopic glioma induced tumor xenografts treated with TMZ and FU, both individually and in combination for a period of 175 days. The dual-drug combination bestowed a significant overall survival advantage in comparison to tumor-control and individual treatment groups, *** $p<0.001$, when compared with that of tumor-control.

Evaluation of organ-based toxicity induced by individual and dual-drug combination on glioma xenografts

Following assessment of the histopathological effect of the individual and dual- drug combinations on the brain tissues of the glioma-induced xenografts, we were interested to examine if this systemic delivery had any adverse effects on the vital organs of the xenografts. Hence, histopathological study was performed on vital organs such as heart, lungs, liver, spleen, pancreas and kidney (Figure16-I and II). Interestingly, photomicrographs of the heart and lungs of the individual and dual-drug treated rats depicted cardiac muscle fibers and normal alveolar structures without any inflammatory lesions. Likewise, liver tissue sections of the individual and dual-drug treated rats depicted visible and distinct hepatocytes arranged in typical pattern and did not portray any signs of necrosis, hemorrhagic lesions or any fatty acid deposits. Similarly, histological sections of pancreas and spleen from all of the treatment groups did not exhibit any gross pathological changes (Figure 16-I and II). Photo micrographic sections of kidney of the treatment groups revealed no such morphological changes. All nephrons depicted visible nucleolus, without any necrotic infiltrations, bleeding or degeneration. Both the proximal and

distal tubules appeared normal without any signs and symptoms of abnormal lesion or atrophies formation. Overall, our histopathological analysis revealed that the oral administration of these drugs both individually and in combination while inducing pathological effect to the tumor tissues, was not toxic to the other vital organs of glioma-induced xenografts (Figure 16-I and II).

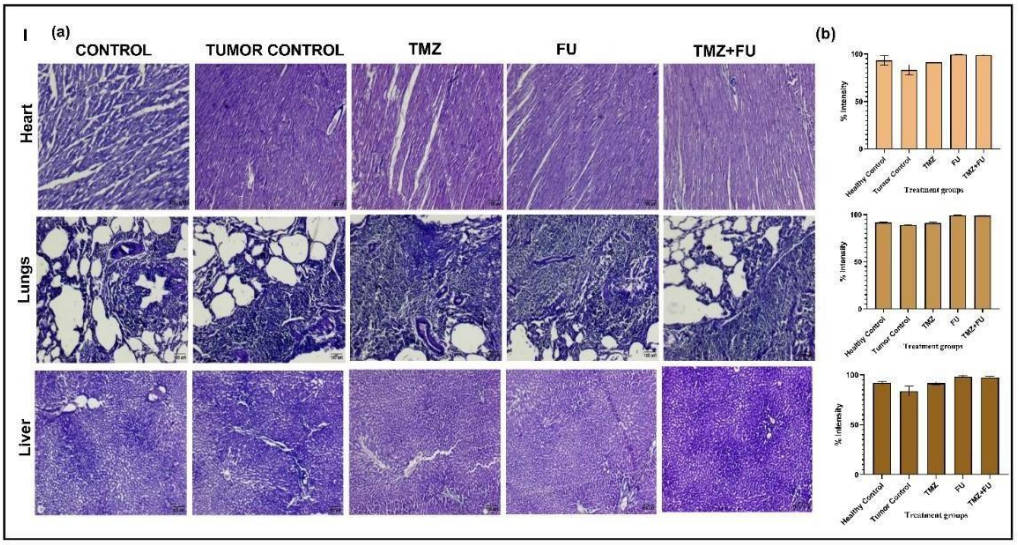

Figure 16-I: (a) Histopathological alterations following administration of the drugs on the vital organs such as heart, lungs, liver, pancreas, spleen and kidney were quantified at 40x magnifications by inverted microscope.
(b) Quantitative data based on the cellularity index was obtained employing ImageJ. Data are represented in terms of Mean ± SD, n=3.

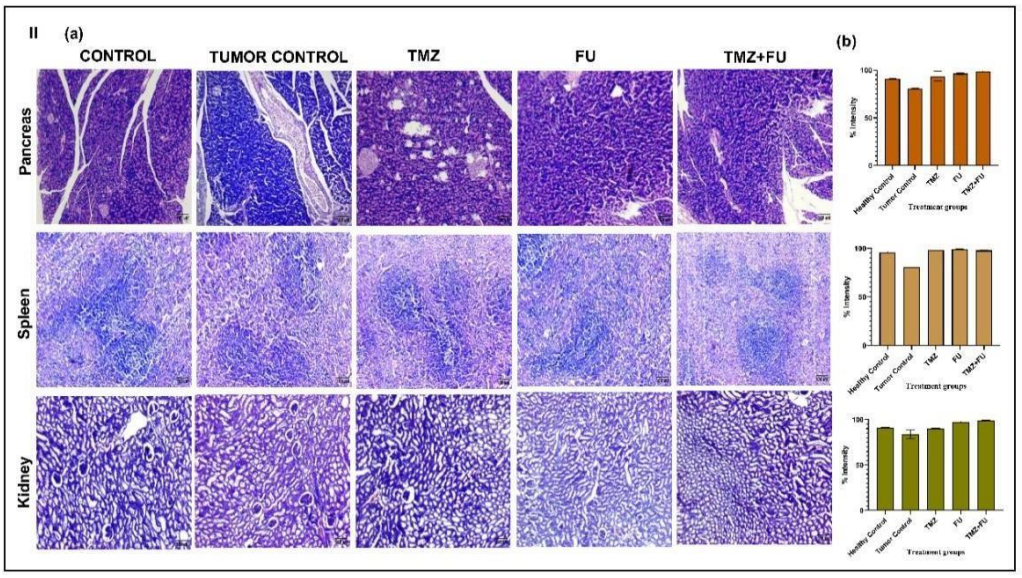

Figure 16-II: (a) Histopathological alterations following administration of the drugs on the vital organs such as heart, lungs, liver, pancreas, spleen and kidney were quantified at 40x magnifications by inverted microscope
(b) Quantitative data based on the cellularity index was obtained employing ImageJ. Data are represented in terms of Mean ± SD, n=3.

Assessment of the ultrastructural changes induced by individual and dual- drug combination in glioma xenografts

Following elucidation of the histopathological effects of the dual-drug combination (TMZ+FU) on the brain tissues and the vital organs, we were interested to determine the ultrastructural variations associated under each of the experimental groups by SEM. While the brain tissue of healthy control/control (Group I) rats depicted a smooth dorsal surface and normal pattern of lamellar projections, the tumor-control (Group II) brain tissues revealed multiple undulating patterns with maximal number of grooves and ridges of an average size of 0.20 µm, irregular patterns of microvili, ruffling and lamellar projections from the membrane (Figure 17-I and II). Interestingly, the dual-drug combination (TMZ+FU) depicted smoothen patterns of microvilli along with the lesser number of grooves, ridges (10, Figure 17-II a) or hollow bodies formation (average size less than 0.05µm, Figure 17-II b), in comparison to tumor-control and individual treatment groups. As individual drugs, though, TMZ and FU (Figure 17-I c and d, IIa and b) exhibited a modest effect on the ultrastructural changes, they were not as effective as the dual-drug combination. Thus, our SEM analysis results suggested that the dual-drug combination (TMZ+FU) had largely restored structural alterations in comparison to tumor-control and individual drug treatment groups and had bestowed maximum ultrastructural integrity at surface level (Figure 17-Ie and II a and b).

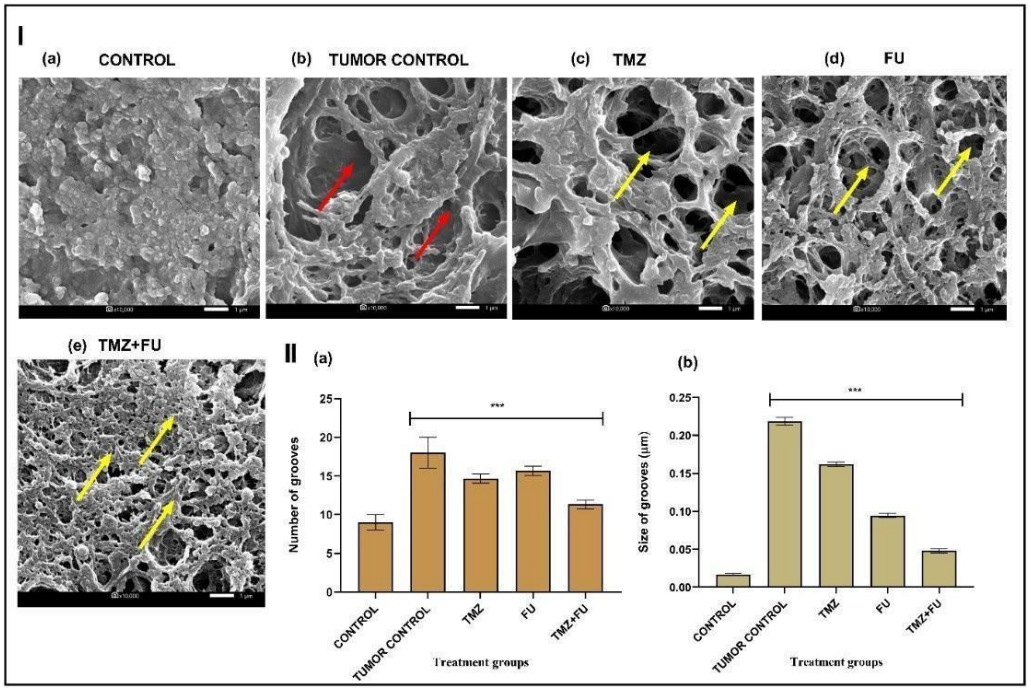

Figure 17: Scanning electron micrograph images of rat brain tissues against different experimental groups was observed at 10,000x. Red arrows indicates a higher no. of grooves formation and altered morphology whereas yellow arrows indicate restoration of the surface morphology, wherein, the dual-drug (TMZ+FU) exhibited elevated levels of surface restoration as compared to individual treatment groups; II (a) and (b) indicated the number and size of grooves formed against each of the experimental groups, respectively.

Morphological effects of the individual and dual-drug combination on inflammatory markers in glioma xenografts

Following elucidation of the ultrastructural alterations imposed by the dual- drug combination (TMZ+FU) on the glioma-induced xenografts; we then elucidated the underlying molecular mechanism using IHC analysis. As depicted in Figure 18-I and II, our IHC results revealed that the dual-drug combination of TMZ+FU (Group V) exhibited reduced expression of inflammatory molecules as per the IRS score-IL-6 (0), TLR4 (0), JAK2 (1), STAT3 (0), IFN-γ (0) and NOS2 (1) in comparison to tumor-control significantly ($p<0.001$, Table 6). However, individually, TMZ and FU treated rats had depicted moderate reduction in expression of these molecules and they were not as significant as the dual-drug combination (Figure 18-Iand II). Thus from our mechanistic studies, the dual-drug combination had induced ultrastructural changes, via modulation of inflammatory markers at morphological level.

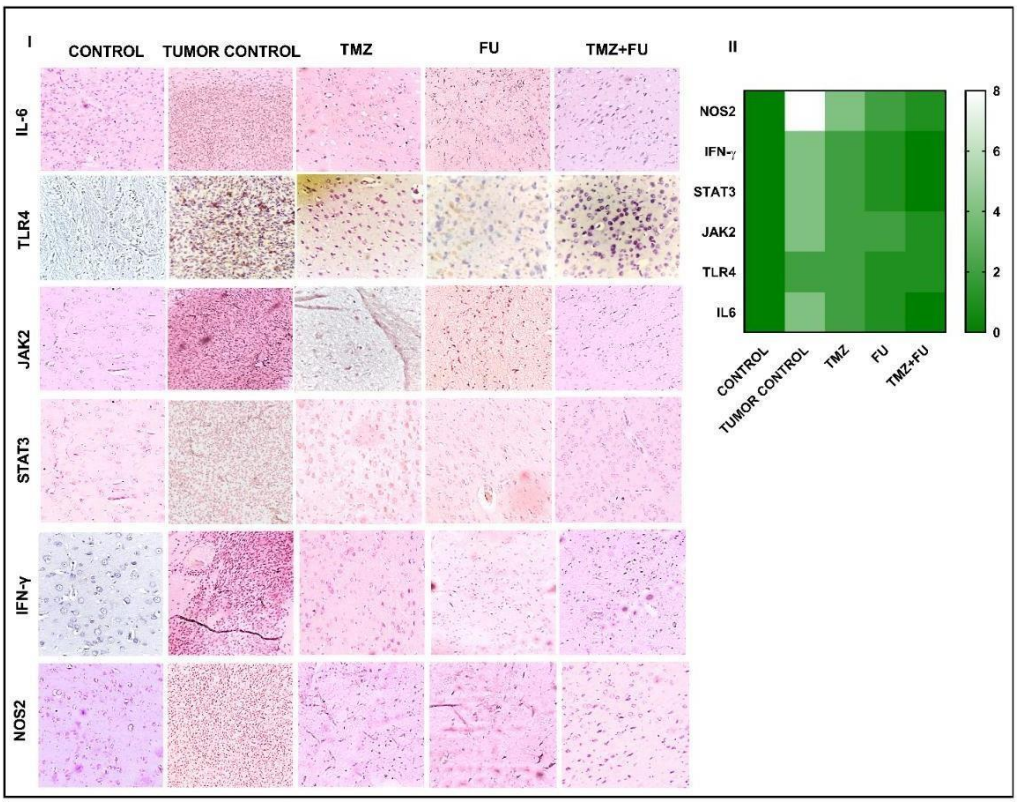

Figure 18: Alterations in expression of the inflammatory molecules against each of the experimental groups (I) Cytoplasmic positivity for IL-6, TLR4, JAK2, STAT3, IFN-γ and NOS2 in glioma induced brain tissues of various experimental groups were detected by IHC (II) Expression analysis of inflammatory molecules against each of experimental groups represented as heat-map.

Table 6: Immunoreactive scores (IRS) enlisting intensity and percentage of positive cells obtained for the inflammatory markers against each of the experimental groups.

Inflammatory Molecules	**Intensity (0-3)**	**Percentage of cells positive (0-4)**	**Immunoreactive score (IRS=**intensity × percentage of positive cells**)**
IL-6			
Control	0	0	0
Tumor Control	2	2	4
TMZ	2	1	2
FU	1	1	1
TMZ+FU	1	0	0
TLR4			
Control	0	0	0
Tumor Control	2	1	2
TMZ	2	1	2
FU	1	1	1
TMZ+FU	0	1	0
JAK2			
Control	0	0	0
Tumor Control	2	2	4
TMZ	2	1	2
FU	1	2	2
TMZ+FU	1	1	1

STAT3B			
Control	0	0	0
Tumor Control	2	2	4
TMZ	1	2	2
FU	1	1	1
TMZ+FU	0	0	0
IFN-γ			
Control	0	0	0
Tumor Control	2	2	4
TMZ	1	2	2
FU	1	1	1
TMZ+FU	1	0	0
NOS2			
Control	0	0	0
Tumor Control	2	4	8
TMZ	2	2	4
FU	1	2	2
TMZ+FU	1	1	1

7. Discussion

About 40% of intracranial tumors are gliomas, which frequently have a poor prognosis and a dismal survival rate. The gold-standard medicine for gliomas, TMZ, is used with radiotherapy and chemotherapy as part of the most modern therapy at the moment. Though TMZ had been hailed as a significant breakthrough as a single treatment, chemo-resistance has caused it to lose some of its therapeutic effectiveness over time. This puts forth a vital need for effective therapeutic strategies. Besides, several preclinical studies had showed that employing mono-therapeutic agents to target glioma were not efficacious as well as not associated with a significant patient outcome. This way, combination therapy has become the cornerstone of the current scenario, as it can bring about synergistic growth inhibitory effect while focusing on multiple gene targets at the same point. For instance, Resveratrol, a polyphenolic substance, inhibited self-renewal and tumor-initiating capacity of patient derived glioma stem cells via downregulation of p53/p21 and Nanog genes, involved in retention of stemness (37). Likewise, quercetin, a natural flavonoid compound exerted anti-invasive and anti-migratory effects via downregulation of GSK3β/β-catenin/ZEB1 signalling pathway in glioma cells. Above all, it has been suggested that combining TMZ with natural or synthetic derivatives would result in a contemporaneous dosage decrease and be an effective strategy for treating glioma because TMZ is linked to significant cytotoxic effects.

One of the key elements in the pathogenesis of glioma that contributes to tumour proliferation and sustenance, hence increasing cell development in glioblastoma, are inflammatory cytokines. Interleukin-6 (IL-6), an autocrine and paracrine cytokine that promotes inflammation, has effects on glioma that advance the tumour. It binds to the glycoprotein complex 130 (gp130 complex) or the interleukin-6 receptor (IL-6R), which activates the Janus kinases (JAK) -STAT3 and has direct effects on tumour cells. In most cancer types, including GBM, STAT3, a member of the transcriptional factor family, is implicated in proliferation, inflammation, and tumorigenesis. The expression of nitric oxide synthase isoform 2 (NOS2), which results in the synthesis of nitric oxide, can be induced by inflammation caused by the binding of the toll-like receptor (TLR-4).

Previously, TMZ and FU have been shown to have profound anti-proliferative and growth-inhibitory effects on a variety of cancer cells. According to those results, the dual-drug combination (TMZ+FU) was found to be non-toxic in normal cells in the current study; however, when given to glioma cells, the drugs significantly inhibited glioma cell proliferation compared to their individual counterparts (Figure 4). This could be related to the interaction between anti-proliferative impact of TMZ and growth inhibitory potency of FU. Additionally, we evaluated the combination index for the dual-drug

combination to see if such an effective anti-proliferative impact was synergistic. We found that on average, 172.105-fold reduction of TMZ and 1.18-fold reduction of FU were sufficient to induce the median effect, while administering the drugs as a dual-drug combination. Moreover, the dual-drug combination along with individual drugs had a higher SI index, suggesting that the dual-drug combination selectively inhibited glioma cell growth (Table 3). Obtaining this synergistic anti-proliferative effect within such reduced drug dosage, would help to improve glioma prognosis and uphold patient survival.

Proliferation and migration in glial tumours are mutually exclusive, which is an interesting observation. Glioma cells "go/migrate" and "re-settle" to "grow/proliferate" in a flexible environment as a result of changes in the tumour microenvironment. This "Go and grow" effect, which encourages tumorigenicity, is crucial in gliomas. Therefore, it is conceivable that finding chemotherapeutic medicines that block the "Go" of glioma might aid in halting tumour cell migration, which in turn would decrease glioma proliferation. In a study by Yan *et al* reported that TMZ exerted anti-tumor effects in U-87MG cells by restricting cell migration (65). Also, previous study findings reported that FU halted proliferation and migration in lung (66), liver (67) and breast cancer cell lines (68). In accordance with these findings, our results revealed that both the drugs had potent anti-migratory effect against glioma. In addition, administration of the dual-drug cocktail has sustained the cell-free space to a significant level, thereby signifying the synergistic anti-migratory effects in suppressing glioma proliferation (Figure 5).

The anti-migratory effect of this dual-drug cocktail would be due to either of the possible mechanisms: suppression of matrix metalloproteinases (MMPs) or upregulated expression of epithelial cadherin (E-cadherin), or via downregulation of transforming growth factor beta (TGF-β). Therefore, we postulate that, as previous study findings state TMZ and FU regulate the expression of the migration parameters in different cancer cells. However, profound molecular analysis is required to conclusively determine if the anti-migratory effect of this combinatorial treatment was due to the suppression of MMP's or TGF-β. The anti-proliferative and anti-migratory effects of the combinatorial drug treatment might be due to induction of apoptosis. In this perception, our dual-drug combination (TMZ+FU) exerted apoptosis in terms of nuclear and cytoplasmic alterations, which might be triggered due to activation of apoptotic signaling pathways, in comparison to control and individual-drug-treated experimental groups.

The majority of cancer cells, including GBM, exhibit apoptosis evasion and progress to a high grade of malignancy that might lead to therapeutic resistance. Since their precise mechanism of action has not been completely established, one of the exciting issues encountered in the field of developing anti-glioma

drugs is the restoration of the apoptotic pathway by therapeutic targets. It is widely accepted that cascades of caspase-mediated events play a major role in the transmission of cell death by apoptosis. From the perspective of anti-cancer treatments, caspases are frequently used as chemotherapeutic or chemo-preventive targets. The majority of anti-cancer drugs generated from marine resources have been found to activate caspase-3 thereby triggering apoptosis.

According to previous studies, TMZ could trigger apoptosis through the non-canonical dependent mitochondrial translocation of STAT3 (79). By a related investigation, STAT3 inhibition increases the sensitivity of glioblastoma to TMZ by downregulation of MGMT expression (80). On the other hand, FU was also understood to promote autophagy and trigger apoptosis through JAK/STAT3 activation (81). Additionally, p-STAT3 was demonstrated to be downregulated by FU, which caused the liver cancer cell line HepG2 to undergo apoptosis (82). According to these results, we found that the dual drug combination of TMZ and FU dramatically increased caspase-3 expression when compared to the groups that received only one drug or the control group. Thereof, we postulate that the combinatorial treatment of TMZ and FU augmented apoptosis by elevating the levels of caspase-3, possibly by down regulating the expression of JAK/STAT3 (Figure 10).

In addition, molecular docking was carried out to clarify the potential binding mechanism of each of these ligands, TMZ, FU, MTIC, and AIC, with the pro-inflammatory targets, IL6, TLR4, JAK2, STAT3, IFN-γ, and NOS2. Docking of TMZ, MTIC, AIC, and FU in the target proteins' active sites was examined using variables such Glide-based binding energy, hydrogen bonds, π-cation interactions, and salt bridge interactions. Comparing FU-IL6 to other ligand-IL6 complexes, the binding energy showed that it had the highest binding energy (Figure 11 and 12). According to simulation studies, all of the complexes (IL6-TMZ, MTIC, and AIC) were stable during the 20,000 ps run time period, which may have been caused by the creation of H-bonds.

Furthermore, we found that the strongest binding energies of (TLR4, JAK2 and STAT3)-MTIC; (IFN-γ and NOS2)-AIC are consistent with strong binding (Figure 11 and 12). Major interactions between STAT3-MTIC and AIC, NOS2-TMZ and MTIC complexes were discovered. Apart from H-bonds, salt bridges, and л-cation interactions may also contribute to the overall stability of these complexes, as evidenced by the creation of salt bridges between (TLR4-TMZ, MTIC, and AIC; JAK2-TMZ and AIC; STAT3-TMZ and AIC; IFN-γ AIC; NOS2-AIC) except IL-6. Following previously reported findings, non-covalent contacts such as salt bridges and л-cation interactions may exhibit stronger interactions than H-bonds. It's interesting to note that, except FU, MTIC, AIC, and TMZ all took part in salt bridge and л-cation interactions in a majority of the targets (Figures 11 and 12).

This could be accounted for by the existence of L-fucose and sulfate ester groups in FU, which may contribute to its cytotoxic and anti-cancer activity, in contrast to the imidazole and triazene rings present in TMZ and its metabolites, which allow for the formation of additional non-covalent form of interactions and result in conformational changes in the targets of inflammation.

To determine the anti-glioma efficacy of this dual-drug cocktail at the translationallevel, employing an orthotopic glioma-induced animal model, we looked at the synergistic anti-glioma efficacy of a dual-drug combination of TMZ and FU, an active substance from brown algae. This study was an extension of our earlier *in vitro* and computational research, in which we found that the combination of TMZ+FU successfully modulated the JAK/STAT and IL-6/TLR4 signaling pathway, leading to cell death.

There are a few factors perceived that hinder the growth of validating anti-cancer drugs towards reaching the patient setting, among which, is the lack of a proper experimental setup to validate their efficacy *in vivo*. Hence, to gain a clear-cut idea of the possible anti-tumor efficacy of the dual-drug combination against glioma, an orthotopic glioma model was established. As compared to the tumor control group, which possessed a majority of cells that were actively dividing and had pleomorphic nuclei and pseudo-palisading necrotic sites, the histopathological analysis of the brain tissues showed a significant reduction in the tumor's cellularity and inflammation after administration of the dual-drug combination. This outcome was in accordance with earlier research where TMZ and FU, used as separate medications, had successfully decreased tumor cellularity in glioma-induced xenografts (Figure 14). This outcome was consistent with our *in vitro* and *in silico* results, which indicated that TMZ+FU and its active metabolites showed strong binding stability to the inflammatory targets.

Following verifying the pathogenic effect, we investigated whether administering this dual-drug combination (TMZ+FU) may extend the glioma-induced xenografts' overall survival. This is because, despite significant advancements in therapeutic approaches that have stemmed the spread of gliomas, the outlook overall is still bleak. A marine sulfated polysaccharide called H3-a1 was previously found to have improved overall survival rates *in vivo* in ascetic sarcoma and lymphoma patients. Interestingly, it was reported that FU improvised quality of life in most of the cancer patients. Furthermore, in a clinical study by Takahashi *et al*., it was reported that, FU enhancedquality of life in advanced colorectal cancer patients. As a supporting notion, in our study, when compared with the tumor-control wherein all the rats were dead by the 8^{th} week of tumor implantation, the dual-drug treatment (TMZ+FU)had prolonged the life expectancy of the glioma-induced rats to about 23.5 weeks (Figure 15), thereby stating that besides exerting significant pathological effect, the dual-drug treatment was able to prolong the overall survival of glioma-induced xenografts.

To affirm if the histopathological effect exerted by the dual-drug combination (TMZ+FU) had imposed any side effects on the vital organs of the glioma-induced xenografts, the sections of the liver, lungs, heart, spleen, pancreas, and kidney were assessed by H&E staining. Interestingly, none of the sections depicted any signs of tissue inflammation, hemorrhage, or necrosis. These findings coincide with the previously reported studies, wherein, individually, TMZ and FU exhibited no morphological changes in the vital organs (37, 38, 39). Thus, systemic delivery of this dual-drug cocktail, which induces a potent histopathological effect to the glioma-induced brain tissues, wasnon-toxic to vital organs of the xenografts (Figure 16-I and II).

On grounds of these observations, we were interested to elucidate if this dual- drug combination (TMZ+FU) was associated with the potency to exhibit any changes to the glioma-induced xenografts at morphological and ultrastructural level. Hence, SEM analysis was carried out wherein we perceived ultrastructural morphological alterations in terms of microvilli appearance. Surface microvilli is a hallmark feature of mesothelial (72), epithelial cells (73) and lymphocytes (74). Alteration in appearance of these structures serves as a key factor towards the formation of malignant glial tumors (75). Furthermore, modification of microvilli, blebs and ridges leads to aggravation of the membranous activity and can enhance the invasiveness of glioma. To add on, tumorigenesis of glioma is positively correlated with altered ultra-structures, which might serve as an attractive therapeutic target to combat glioma proliferation (76). As corroboration to this lacuna, we observed that the dual-drug combination (TMZ+FU) had restored the morphological alterations in comparison to tumor control group and individual treatment groups (Figure 17). This finding was in line with the previous research by Bakar *et al.* wherein the ethanolic extract of red seaweed *Eucheuma cottonii* had restored the ultrastructural changes to normal level *in vivo,* in a breast tumor model (77). Thus, our SEM findings suggested that while reducing the tumor cellularity, the dual-drug combination was able to restore the ultrastructural changes in the glioma-induced xenografts, thereby, providing a hint to assess the underlying molecular mechanism.

As a continuation of assessment of the ultra-structural modifications, in order to gain molecular insights of this dual-drug combination (TMZ+FU) against glioma, IHC was performed. It is well known fact that molecular dysfunction of PI3K/AKT, RAS/RAF, JAK/STAT3, IL-6/TLR4, leads to tumorigenesis of glioma. Among them, the JAK/STAT3 and IL-6/TLR4 pathway has been reported to contribute to glioma progression and are strongly correlated with modulation of histological patterns in glioma. Hence, in order to predict the therapeutic outcome of this dual-drug combination (TMZ+FU) at translational level, we examined the expression levels of these inflammatory markers. Previously, Takahashi *et al.*, had reported that FU had induced anti-inflammatory effects in advanced colorectal cancer patients via down-regulation of inflammatory cytokines and improved overall survival. Also, activation of JAK/STAT3 signaling was reduced by oral administration

of FU in a prostate cancer xenograft model. Additionally, FU exhibited anti-inflammatory effects in colorectal cancer xenograft model by down-regulation of inflammatory markers such as TNF-α IL-6 and IL-1β. Further, the anti-inflammatory effects of FU were evident in B16 melanoma and rat mammary adenocarcinoma model. Consistent with those findings, in our study, the dual-drug combination (TMZ+FU) had significantly down-regulated the expression of these inflammatory markers ($p<0.001$), when compared to their efficacy as individual drugs (Figure 18-A and B). Thus, our morphological analysis revealed that while restoring the ultra-structural changes, the dual-drug combination had reduced the inflammation in glioma-induced xenografts via modulation of the JAK/STAT3 and IL-6/TLR4 pathways.

It is well-established that the pathogenesis of glioma is not restricted to growth and proliferation, but also other pathological features such as inflammation and induction of ultra-structural changes. Taken together, the results of the current study emphasize that the dual-drug combination (TMZ+FU) could efficiently reduce the tumor pathogenesis and prolong the overall survival of glioma induced xenografts. Our morphological studies had highlighted that administration of TMZ+FU can restore the morphology of the xenografts via modulation of JAK/STAT3 and IL-6/TLR4 signaling cascade. However, there are certain limitations in the current study. Firstly, the effect of this dual-drug combination on inflammatory markers is assessed at morphological level. Hence, futuristic studies focusing on the assessment of these markers at transcriptional and translational level would justify the findings of this research. Secondly, assessing the potency in immune-compromised models using TMZ- resistant cell lines would provide a clear-cut idea on the anti-glioma efficacy of this dual-drug combination, which is to be accomplished in mere future.

8. SUMMARY & CONCLUSION

Glioma represents the aggressive and dreadful form of brain tumor, with a dismal prognosis. The current standard-of care remains surgical resection, following radiotherapy and chemotherapy with alkylating agent, i.e, Temozolomide (TMZ). Despite the tripartite therapy, glioma patients survive with poor prognosis. Drug repurposing employs existing medications with known pharmacokinetics and toxicity profile. In recent years, marine natural products have gained increasing interests owing to its potential pharmacological properties. In view of the desperate need for alternate therapies against glioma, the current study had investigated the efficacy of

combination of a synthetic and natural derivative of marine origin (TMZ and FU, respectively). Interestingly, the dual-drug cocktail (TMZ+FU) exerted anti-glioma effects by restricting growth, proliferation, migration mediated via downregulation of inflammatory molecules with concurrent upregulated expression of apoptosis. The active metabolites of TMZ, i.e, MTIC and AIC, are one of the key contributing factors of the cytotoxic effects exerted by co-administration of TMZ and FU against the inflammatory markers in glioma. Furthermore, as a step forward to translate the *in vitro* and *in silico* findings, *in vivo* experimental studies were performed, wherein, the dual-drug cocktail abrogated tumor growth accompanied by an increment in the overall survival rate of the glioma-induced xenografts. Further, the novel combination of TMZ and FU didn't induce any toxicity among the vital organs and restored the ultrastructural patterns in the glioma-induced xenografts animal model, justifying the selective anti-tumor efficacy of this cocktail against glioma via downregulation of inflammatory markers namely IL6/TLR4 and JAK/STAT3. Although this dual-drug cocktail exhibited synergistic anti-tumor effects *in vitro*, *in silico*, and *in vivo* experimental setup, detailed molecular insights are a prerequisite of the present study before translating from bench to bedside successfully.

9. REFERENCES

1. Nabors LB, Ammirati M, Bierman PJ, Brem H, Butowski N, Chamberlain MC, et al. Central Nervous System Cancers. J Natl Compr Canc Netw. 2013 Sep 1;11(9):1114–51.

2. Khosla D. Concurrent therapy to enhance radiotherapeutic outcomes in glioblastoma. Ann Transl Med. 2016 Feb;4(3):54.

3. Kirtonia A, Gala K, Fernandes SG, Pandya G, Pandey AK, Sethi G, et al. Repurposing of drugs: An attractive pharmacological strategy for cancer therapeutics. Semin Cancer Biol. 2021 Jan; 68:258–78.

4. Nowak-Sliwinska P, Scapozza L, Ruiz i Altaba A. Drug repurposing in oncology: Compounds, pathways, phenotypes and computational approaches for colorectal cancer. Biochim Biophys Acta Rev Cancer. 2019 Apr;1871(2):434-454.

5. Lin S, Chang C, Hsu C, Tsai M, Cheng H, Leong MK, et al. Natural compounds as potential adjuvants to cancer therapy: Preclinical evidence. Br J Pharmacol. 2020 Mar;177(6):1409–23.

6. Shinde P, Banerjee P, Mandhare A. Marine natural products as source of new drugs: a patent review (2015-2018). Expert Opin Ther Pat. 2019 Apr;29(4):283– 309.

7. Lichota A, Gwozdzinski K. Anticancer Activity of Natural Compounds from Plant and Marine Environment. Int J Mol Sci. 2018 Nov 9;19(11):3533.

8. Yang H, Zhao H, Dong X, Yang Z, Chang W. Tomentosin induces apoptotic pathway by blocking inflammatory mediators via modulation of cell proteins in AGS gastric cancer cell line. J Biochem Mol Toxicol. 2020 Aug;34(8):e22501.

9. Li B, Lu F, Wei X, Zhao R. Fucoidan: Structure and Bioactivity. Molecules. 2008 Aug 12;13(8):1671–95.

10. Rui X, Pan HF, Shao SL, Xu XM. Anti-tumor and anti-angiogenic effects of Fucoidan on prostate cancer: possible JAK-STAT3 pathway. BMC Complementary and Alternative Medicine. 2017 Aug 1;17(1):378.

11. Hsu HY, Hwang PA. Clinical applications of fucoidan in translational medicine for adjuvant cancer therapy. Clinical and Translational Medicine. 2019;8(1):e15.

12. Liao CH, Lai IC, Kuo HC, Chuang SE, Lee HL, Whang-Peng J, et al. Epigenetic Modification and Differentiation Induction of Malignant Glioma Cells by Oligo- Fucoidan. Mar Drugs. 2019 Sep 8;17(9):525.

13. Hanif F, Muzaffar K, Perveen K, Malhi SM, Simjee SU. Glioblastoma Multiforme: A Review of its Epidemiology and Pathogenesis through Clinical Presentation and Treatment. Asian Pac J Cancer Prev.

2017;18(1):3–9.

14. Kleihues P, Louis DN, Scheithauer BW, Rorke LB, Reifenberger G, Burger PC, et al. The WHO Classification of Tumors of the Nervous System. Journal of Neuropathology & Experimental Neurology. 2002 Mar 1;61(3):215–25.

15. Kaifi R. A Review of Recent Advances in Brain Tumor Diagnosis Based on AI-Based Classification. Diagnostics (Basel). 2023 Sep 20;13(18):3007.

16. Bhowmik A, Khan R, Ghosh MK. Blood Brain Barrier: A Challenge for Effectual Therapy of Brain Tumors. Biomed Res Int. 2015; 2015:320941.

17. Perry A, Wesseling P. Histologic classification of gliomas. In: Handbook of Clinical Neurology]. Elsevier; 2016. p. 71–95.

18. Haque A, Banik NL, Ray SK. Molecular alterations in Glioblastoma potential targets for immunotherapy. Prog Mol Biol Transl Sci. 2011; 98:187–234.

19. Larjavaara S, Mäntylä R, Salminen T, Haapasalo H, Raitanen J, Jääskeläinen J, et al. Incidence of gliomas by anatomic location. Neuro Oncol. 2007 Jul;9(3):319– 25.

20. Olden K, White SL. Health-Related Disparities: Influence of Environmental Factors. Medical Clinics of North America. 2005 Jul;89(4):721–38.

21. Ostrom QT, Bauchet L, Davis FG, Deltour I, Fisher JL, Langer CE, et al. The epidemiology of glioma in adults: a "state of the science" review. Neuro- Oncology. 2014 Jul 1;16(7):896–913.

22. Dymova MA, Kuligina EV, Richter VA. Molecular Mechanisms of Drug Resistance in Glioblastoma. Int J Mol Sci. 2021 Jun 15;22(12):6385.

23. Anitha T, Kuduvalli S, Biswas I, Vignesh M, Mangaiyarkarasi N. Insights into Molecular Mediators of Oxidative Stress and Inflammation in Glioblastoma Multiforme. SBV Journal of Basic, Clinical and Applied Health Science. 2021 Feb 9;3:137–43.

24. Chien LN, Gittleman H, Ostrom QT, Hung KS, Sloan AE, Hsieh YC, et al. Comparative Brain and Central Nervous System Tumor Incidence and Survival between the United States and Taiwan Based on Population-Based Registry. Front Public Health. 2016 Jul 21;4:151.

25. Rajesh Y, Pal I, Banik P, Chakraborty S, Borkar SA, Dey G, et al. Insights into molecular therapy of glioma: current challenges and next generation blueprint. Acta Pharmacol Sin. 2017 May;38(5):591–613.

26. Furtado FS, Wu MZ, Esfahani SA, Ferrone CR, Blaszkowsky LS, Clark JW, et al. Positron Emission Tomography/Magnetic Resonance

Imaging (PET/MRI) Versus the Standard of Care Imaging in the Diagnosis of Peritoneal Carcinomatosis. Ann Surg. 2023 Apr 1;277(4):e893–9.

27. Seaman ME, Contino G, Bardeesy N, Kelly KA. Molecular imaging agents: impact on diagnosis and therapeutics in oncology. Expert Rev Mol Med. 2010 Jul 15;12:e20.

28. Li D, Patel CB, Xu G, Iagaru A, Zhu Z, Zhang L, et al. Visualization of Diagnostic and Therapeutic Targets in Glioma With Molecular Imaging. Front Immunol. 2020 Oct 30;11:592389.

29. Wei W, Ni D, Ehlerding EB, Luo QY, Cai W. PET imaging of receptor tyrosine kinases in cancer. Mol Cancer Ther. 2018 Aug;17(8):1625–36.

30. Kołodziej M, Bober B, Saracyn M, Kamiński G. The Role of PET/CT with 11C-Methionine in contemporary nuclear medicine. Wiad Lek. 2020;73(9 cz. 2):2076–9.

31. Marais S, Van Toorn R, Chow FC, Manesh A, Siddiqi OK, Figaji A, et al. Management of intracranial tuberculous mass lesions: how long should we treat for? Wellcome Open Res. 2020 Feb 26;4:158.

32. Kamiya-Matsuoka C, Gilbert MR. Treating recurrent glioblastoma: an update. CNS Oncol. 2015 Mar;4(2):91–104.

33. Singh N, Miner A, Hennis L, Mittal S. Mechanisms of temozolomide resistance in glioblastoma - a comprehensive review. Cancer Drug Resist. 2021 Mar 19;4(1):17–43.

34. Villalva C, Cortes U, Wager M, Tourani JM, Rivet P, Marquant C, et al. O6- Methylguanine-methyltransferase (MGMT) promoter methylation status in glioma stem-like cells is correlated to temozolomide sensitivity under differentiation-promoting conditions. Int J Mol Sci. 2012;13(6):6983–94.

35. Persano F, Gigli G, Leporatti S. Natural Compounds as Promising Adjuvant Agents in The Treatment of Gliomas. Int J Mol Sci. 2022 Mar 20;23(6):3360.

36. Almatroodi SA, Almatroudi A, Khan AA, Alhumaydhi FA, Alsahli MA, Rahmani AH. Potential Therapeutic Targets of Epigallocatechin Gallate (EGCG), the Most Abundant Catechin in Green Tea, and Its Role in the Therapy of Various Types of Cancer. Molecules. 2020 Jul 9;25(14):3146.

37. Sato A, Okada M, Shibuya K, Watanabe E, Seino S, Suzuki K, et al. Resveratrol promotes proteasome-dependent degradation of Nanog via p53 activation and induces differentiation of glioma stem cells. Stem Cell Research. 2013 Jul 1;11(1):601–10.

38. Nakada M, Kita D, Watanabe T, Hayashi Y, Teng L, Pyko IV, et al. Aberrant Signaling Pathways in Glioma. Cancers (Basel). 2011 Aug 10;3(3):3242–78.

39. Mostofa AGM, Punganuru SR, Madala HR, Al-Obaide M, Srivenugopal KS. The Process and Regulatory Components of Inflammation in Brain Oncogenesis. Biomolecules. 2017 Mar 27;7(2):34.

40. Galvão RP, Zong H. Inflammation and Gliomagenesis: Bi-Directional Communication at Early and Late Stages of Tumor Progression. Curr Pathobiol Rep. 2013 Mar 1;1(1):19–28.

41. Gopinath A, Collins A, Khoshbouei H, Streit WJ. Microglia and Other Myeloid Cells in Central Nervous System Health and Disease. J Pharmacol Exp Ther. 2020 Oct;375(1):154–60.

42. Verdeil G, Lawrence T, Schmitt-Verhulst AM, Auphan-Anezin N. Targeting STAT3 and STAT5 in Tumor-Associated Immune Cells to Improve Immunotherapy. Cancers (Basel). 2019 Nov 21;11(12):1832.

43. Tran AN, Boyd NH, Walker K, Hjelmeland AB. NOS Expression and NO Function in Glioma and Implications for Patient Therapies. Antioxid Redox Signal. 2017 Jun 10;26(17):986–99.

44. Shi Y. Caspase activation, inhibition, and reactivation: A mechanistic view. Protein Sci. 2004 Aug;13(8):1979–87.

45. Valtorta S, Salvatore D, Rainone P, Belloli S, Bertoli G, Moresco RM. Molecular and Cellular Complexity of Glioma. Focus on Tumour Microenvironment and the Use of Molecular and Imaging Biomarkers to Overcome Treatment Resistance. Int J Mol Sci. 2020 Aug 6;21(16):5631.

46. Zoete V, Grosdidier A, Michielin O. Docking, virtual high throughput screening and in silico fragment-based drug design. J Cell Mol Med. 2009 Feb;13(2):238– 48.

47. Lee SY. Temozolomide resistance in glioblastoma multiforme. Genes Dis. 2016 May 11;3(3):198–210.

48. Qian X, Song H, Ming G li. Brain organoids: advances, applications and challenges. Development. 2019 Apr 15;146(8):dev166074.

49. Akter F, Simon B, de Boer NL, Redjal N, Wakimoto H, Shah K. Pre-clinical tumor models of primary brain tumors: Challenges and Opportunities. Biochim Biophys Acta Rev Cancer. 2021 Jan;1875(1):188458.

50. Yang H, Zhao H, Dong X, Yang Z, Chang W. Tomentosin induces apoptotic pathway by blocking inflammatory mediators via modulation of cell proteins in AGS gastric cancer cell line. J Biochem Mol Toxicol. 2020 Aug;34(8):e22501.

51. Fischer AH, Jacobson KA, Rose J, Zeller R. Hematoxylin and Eosin Staining of Tissue and Cell Sections. Cold Spring Harb Protoc. 2008 May;2008(5):pdb.prot4986.

52. Ghasemian M, Mahdavi M, Zare P, Ali Hosseinpour Feizi M. Spiroquinazolinone- induced cytotoxicity and apoptosis in K562 human leukemia cells: alteration in expression levels of Bcl-2 and Bax. J Toxicol Sci. 2015 Feb 1;40(1):115–26.

53. Mandelkow R, Gümbel D, Ahrend H, Kaul A, Zimmermann U, Burchardt M, et al. Detection and Quantification of Nuclear Morphology Changes in Apoptotic Cells by Fluorescence Microscopy and Subsequent Analysis of Visualized Fluorescent Signals. Anticancer Res. 2017 May;37(5):2239–44.

54. Harder E, Damm W, Maple J, Wu C, Reboul M, Xiang JY, et al. OPLS3: A Force Field Providing Broad Coverage of Drug-like Small Molecules and Proteins. J Chem Theory Comput. 2016 Jan 12;12(1):281–96.

55. Muralidharan AR, Selvaraj C, Singh SK, Sheu JR, Thomas PA, Geraldine P. Structure-Based Virtual Screening and Biological Evaluation of a Calpain Inhibitor for Prevention of Selenite-Induced Cataractogenesis in an in Vitro System. J Chem Inf Model. 2015 Aug 24;55(8):1686–97.

56. Abraham MJ, Murtola T, Schulz R, Páll S, Smith JC, Hess B, et al. GROMACS: High performance molecular simulations through multi-level parallelism from laptops to supercomputers. SoftwareX. 2015 Sep 1;1–2:19–25.

57. Singh N, Dalal V, Kumar P. Structure based mimicking of Phthalic acid esters (PAEs) and inhibition of hACMSD, an important enzyme of the tryptophan kynurenine metabolism pathway. International Journal of Biological Macromolecules. 2018 Mar;108:214–24.

58. Baker GJ, Castro MG, Lowenstein PR. Isolation and Flow Cytometric Analysis of Glioma-infiltrating Peripheral Blood Mononuclear Cells. J Vis Exp. 2015 Nov 28;(105):53676.

59. Zhan E, Chu F, Zhao T, Chai Y, Liang H, Song S, et al. Determination of fucoidan in rat plasma by HPLC and its application in pharmacokinetics. Pak J Pharm Sci. 2020 Jan;33(1):1–9.

60. Pozharitskaya ON, Shikov AN, Faustova NM, Obluchinskaya ED, Kosman VM, Vuorela H, et al. Pharmacokinetic and Tissue Distribution of Fucoidan from Fucus vesiculosus after Oral Administration to Rats. Marine Drugs. 2018 Apr;16(4):132.

61. González-Cámpora R, Haynes LW, Weller RO. Scanning electron microscopy of malignant gliomas. A comparative study of glioma cells in smear preparations and in tissue culture. Acta Neuropathol. 1978 Mar 15;41(3):217–21.

62. Vollmann-Zwerenz A, Leidgens V, Feliciello G, Klein CA, Hau P. Tumor Cell Invasion in Glioblastoma. International Journal of Molecular Sciences. 2020 Mar;21(6).

63. Fulda S. Evasion of Apoptosis as a Cellular Stress Response in Cancer. International Journal of Cell Biology. 2010 Feb 18;2010:e370835.

64. Ha ET, Antonios JP, Soto H, Prins RM, Yang I, Kasahara N, et al. Chronic inflammation drives glioma growth: cellular and molecular factors responsible for an immunosuppressive microenvironment. Neuroimmunology and Neuroinflammation. 2014 Aug 28;1:66–76.

65. Yan Y, Xu Z, Dai S, Qian L, Sun L, Gong Z. Targeting autophagy to sensitive glioma to temozolomide treatment. Journal of Experimental & Clinical Cancer Research. 2016 Feb 2;35(1):23.

66. Hsu HY, Lin TY, Wu YC, Tsao SM, Hwang PA, Shih YW, et al. Fucoidan inhibition of lung cancer in vivo and in vitro: role of the Smurf2-dependent ubiquitin proteasome pathway in TGFβ receptor degradation. Oncotarget. 2014 Aug 6;5(17):7870–85.

67. Pan TJ, Li LX, Zhang JW, Yang ZS, Shi DM, Yang YK, et al. Antimetastatic Effect of Fucoidan-Sargassum against Liver Cancer Cell Invadopodia Formation via Targeting Integrin αVβ3 and Mediating αVβ3/Src/E2F1 Signaling. J Cancer. 2019 Aug 27;10(20):4777–92.

68. Li W, Xue D, Xue M, Zhao J, Liang H, Liu Y, et al. Fucoidan inhibits epithelial-to- mesenchymal transition via regulation of the HIF-1α pathway in mammary cancer cells under hypoxia. Oncol Lett. 2019 Jul;18(1):330–8.

69. Mirabdaly S, Elieh Ali Komi D, Shakiba Y, Moini A, Kiani A. Effects of temozolomide on U87MG glioblastoma cell expression of CXCR4, MMP2, MMP9, VEGF, anti-proliferatory cytotoxic and apoptotic properties. Mol Biol Rep. 2020 Feb;47(2):1187–97.

70. Chen MC, Hsu WL, Hwang PA, Chou TC. Low Molecular Weight Fucoidan Inhibits Tumor Angiogenesis through Downregulation of HIF-1/VEGF Signaling under Hypoxia. Mar Drugs. 2015 Jul 17;13(7):4436–51.

71. Alves C, Silva J, Pinteus S, Gaspar H, Alpoim MC, Botana LM, et al. From Marine Origin to Therapeutics: The Antitumor Potential of Marine Algae-Derived Compounds. Frontiers in Pharmacology. 2018;9.

72. Andrews PM, Porter KR. The ultrastructural morphology and possible functional significance of mesothelial microvilli. Anat Rec. 1973 Nov;177(3):409–26.

73. Kasioulis I, Dady A, James J, Prescott A, Halley PA, Storey KG. A lateral protrusion latticework connects neuroepithelial cells and is regulated during neurogenesis. J Cell Sci. 2022 Mar 15;135(6):jcs259897.

74. Majstoravich S, Zhang J, Nicholson-Dykstra S, Linder S, Friedrich W, Siminovitch KA, et al. Lymphocyte microvilli are dynamic, actin-dependent structures that do not require Wiskott-Aldrich syndrome

protein (WASp) for their morphology. Blood. 2004 Sep 1;104(5):1396–403.

75. Baghban R, Roshangar L, Jahanban-Esfahlan R, Seidi K, Ebrahimi-Kalan A, Jaymand M, et al. Tumor microenvironment complexity and therapeutic implications at a glance. Cell Communication and Signaling. 2020 Apr 7;18(1):59.

76. Pibuel MA, Poodts D, Díaz M, Hajos SE, Lompardía SL. The scrambled story between hyaluronan and glioblastoma. J Biol Chem. 2021 Mar 17;296:100549.

77. Bakar NA, Tengku Ibrahim TA, Mohamad Shalan NA, Mohamed S. Changes in rats' breast tumor ultrastructure and immune and messenger RNA responses caused by dietary Seaweed (Kappaphycus alvarezii) extract. J Microsc Ultrastruct. 2017;5(2):70–81.

10. Publications

ORIGINAL ARTICLE

Unveiling the anti-glioma potential of a marine derivative, Fucoidan: its synergistic cytotoxicity with Temozolomide—an in vitro and in silico experimental study

Indrani Biswas[1] · Daisy S. Precilla[1] · Shreyas S. Kuduvalli[1] · Muralidharan Arumugam Ramachandran[2] · S. Akshaya[3] · Venkat Raman[4] · Dhamodharan Prabhu[5] · T. S. Anitha[1,6]

Received: 30 March 2023 / Accepted: 16 October 2023
© King Abdulaziz City for Science and Technology 2023

Abstract
Glioma coined as a "butterfly" tumor associated with a dismal prognosis. Marine algal compounds with the richest sources of bioactive components act as significant anti-tumor therapeutics. However, there is a paucity of studies conducted on Fucoidan to enhance the anti-glioma efficacy of Temozolomide. Therefore, the present study aimed to evaluate the synergistic anti-proliferative, anti-inflammatory and pro-apoptotic effects of Fucoidan with Temozolomide in in vitro and in silico experimental setup. The anti-proliferative effects of Temozolomide and Fucoidan were evaluated on C6 glioma cells by MTT and migration assay. Modulation of inflammatory markers and apoptosis induction was affirmed at the morphological and transcriptional level by dual staining and gene expression. Molecular docking (MD) and molecular dynamics simulation (MDS) studies were performed against the targets to rationalize the inhibitory effect. The dual-drug combination significantly reduced the cell viability and migration of glioma cells in a synergistic dose-dependent manner. At the molecular level, the dual-drug combination significantly down-regulated inflammatory genes with a concomitant upregulation of pro-apoptotic marker. In consensus with our in vitro findings, molecular docking and simulation studies revealed that the anti-tumor ligands: Temozolomide, Fucoidan with 5-(3-Methy1-trizeno)-imidazole-4-carboxamide (MTIC), and 4-amino-5-imidazole-carboxamide (AIC) had the potency to bind to the inflammatory proteins at their active sites, mediated by H-bonds and other non-covalent interactions. The dual-drug combinatorial treatment synergistically inhibited the proliferation, migration of glioma cells and promoted apoptosis; conversely with the down-regulation of inflammatory genes. However, pre-clinical experimental evidence is warranted for the possible translation of this combination.

Keywords Glioma · Drug repurposing · Inflammatory and apoptotic markers · Molecular docking and simulation

Introduction

Glioma, a primary brain tumor arising from multi-step tumorigenesis of glial cells, is often characterized by poor prognosis with a median 5-years survival rate of less than

Indrani Biswas and Daisy S. Precilla have contributed equally to this work.

✉ T. S. Anitha
tsanitha6@pondiuni.ac.in; tsanitha6@gmail.com

[1] Mahatma Gandhi Medical Advanced Research Institute, Sri Balaji Vidyapeeth (Deemed to-be University), Puducherry 607402, India

[2] Department of Visual Neurosciences, Singapore Eye Research Institute, Singapore 169856, Singapore

[4] Thiruvalluvar University, Vellore, Tamil Nadu 632115, India

[5] Centre for Drug Discovery, Department of Biotechnology, Karpagam Academy of Higher Education, Coimbatore 641021, India

[6] Present Address: Department of Biochemistry and Molecular Biology, Pondicherry University, Puducherry 605014, India

Anticancer Original Research Paper

Ultrastructural and immunohistochemical insights on the anti-glioma effects of a dual-drug cocktail in an *in vivo* experimental model

Indrani Biswas, Daisy Precilla S., Shreyas S. Kuduvalli, Bhavani K., Sivachandran R. & Anitha T. S.

Received 30 Aug 2023, Accepted 03 Jan 2024, Published online: 19 Jan 2024

Cite this article https://doi.org/10.1080/1120009X.2024.2302741 Check for updates

Abstract

Glioma coined as 'butterfly tumor' exhibits intense heterogeneity at the molecular and cellular levels. Although, Temozolomide exerted a long-ranging and prevailing therapeutic effect against glioma, albeit it has provided modest survival outcome. Fucoidan, (marine brown algal derivative) has demonstrated potent anti-tumor effects including glioma. Nevertheless, there is paucity of studies conducted on Fucoidan to enhance the anti-glioma efficacy of Temozolomide. The present study aimed to explore the plausible synergistic anti-glioma efficacy of Fucoidan in combination with Temozolomide in an in vivo experimental model. The dual-drug combination significantly inhibited tumor growth in in vivo and prolonged the survival rate when compared with the other treatment and tumor-control groups, via down-regulation of inflammatory cascade- IL-6/T LR4 and JAK/STAT3 as per the immunohistochemistry findings. Furthermore, the ultrastructural analysis indicated that the combinatorial treatment had restored the normal neuronal architecture of glioma-induced rats. Overall, the dual-drug cocktail might enhance the therapeutic outcome in glioma patients.

Keywords: Glioma | temozolomide | fucoidan | inflammation | ultrastructural | immunohistochemistry

Related Rese

People also read

Factors associated dysfunction induc cancer patients: a

Xiao-Chen Wei et

Journal of Chemoth

Published online: 19

Insights into Molecular Mediators of Oxidative Stress and Inflammation in Glioblastoma Multiforme

Indrani Biswas[1], Shreyas S Kuduvalli[2], Mariappan Vignesh[3], Natarajan Mangaiyarkarasi[4], Thirugnanasambandhar S Anitha[5]

Abstract

Glioblastoma multiforme (GBM) is one of the most common aggressive and fatal forms of adult brain tumors. According to WHO classification, GBM is usually classified as a grade IV form of a brain tumor. Glioblastoma multiforme exhibits high intra- and inter-tumoral heterogeneity. Free radical generation in GBM plays a robust role in promoting and inducing inflammatory processes mediated by various signaling pathways mainly focusing on Janus-kinases (JAK). Phosphatidylinositol-3-kinase (PI3K)/AKT/mammalian target of rapamycin (mTOR) stimulates signal transducer activating transcription factor 3 (STAT3) and JNK to induce proinflammatory cytokines, such as, interleukin (IL)-2, IL-6, and IL-8 to aggravate the inflammatory process. This review summarizes the convergence of inflammation and oxidative stress and examines the potential therapeutic targets aimed at the molecular markers in GBM.

Keywords: Glioblastoma multiforme, Inflammation, Molecular markers, Oxidative stress.

SBV Journal of Basic, Clinical and Applied Health Science (2020): 10.5005/jp-journals-10082-02274

Introduction

Glioblastoma multiforme (GBM) is considered to be the most aggressive tumor form of the central nervous system (CNS), with extensive invasion and differentiation.[1] Though GBM is a rare disease with a global incidence of less than 10 per 100,000 people, its poor prognosis with a survival rate of 14–15 months after diagnosis makes it clinically challenging.[2] The difficulty in GBM treatment is usually attributed to several clinical hurdles, such as, failure of drug delivery through the blood–brain barrier, tumor unresponsive to chemotherapy, and development of multidrug resistance by tumor cells.[3]

Several physiological processes which include inflammation, apoptosis, oxidant/antioxidant balance, differentiation, and angiogenesis contribute to GBM.[4] Oxidative stress is one of the major contributors to the pathogenesis of GBM; wherein it triggers lipid peroxidation of cellular membranes, oxidation of proteins, and DNA damage, leading to changes in chromosome structure, genetic mutation, and/or modulation of cell growth.[5] Many reports suggest that intracellular accumulation of reactive oxygen species (ROS) in the mammalian brain is directly responsible for cellular and tissue dysfunction.[6] Excess free radicals generated induce oxidative stress and develop extensive DNA damage, thereby making it a major contributor to GBM development.[7]

Genetic and molecular alterations through multi-step tumorigenesis lead to the development of primary and secondary high-grade glioma, based on clinical, molecular, and pathological characteristics.[8] Primary GBM involves loss of heterozygosity (LOH) of chromosome 10 bearing phosphotensin homolog (PTEN), gene amplification of epidermal growth factor receptor (EGFR), or deletion mutation of EGFR to EGFRvIII and enhanced activity of

[1–5]Central Inter-disciplinary Research Facility (CIDRF), Sri Balaji Vidyapeeth (Deemed to be University), Puducherry, India

Corresponding Author: Thirugnanasambandhar S Anitha, Central Inter-disciplinary Research Facility (CIDRF), Sri Balaji Vidyapeeth (Deemed to be University), Puducherry, India, Phone: +91 9843576675, e-mail: tsanitha6@gmail.com

How to cite this article: Biswas I, Kuduvalli SS, Vignesh M, Mangaiyarkarasi N, Anitha TS. Insights into Molecular Mediators of Oxidative Stress and Inflammation in Glioblastoma Multiforme. J Basic Clin Appl Health Sci 2020;3(4):137–143.

Source of support: Nil

Conflict of interest: None

level mediated, mostly by receptor tyrosine kinase/RAS/mitogen-activated protein kinase (MAPK)/phosphatidylinositol-3-kinase (PI3K) signaling pathway.[10]

Heterogeneity in GBM can be attributed mainly due to: (i) aberrations at genetic and transcriptional level and (ii) molecular markers.[11]

Aberrations at Genetic and Transcriptional Level and Molecular Markers

Gain- or loss-of-function in proto-oncogenes and tumor-suppressor genes has been associated with tumor heterogeneity, including drug resistance. Epidermal growth factor receptor, a transmembrane tyrosine kinase, functions as a critical player involved in proliferation, migration, and cell survival in most